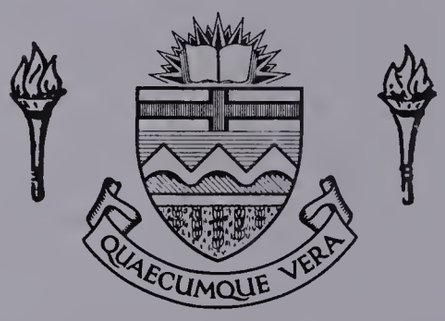

THE UNIVERSITY OF ALBERTA

RELEASE FORM

NAME OF AUTHOR ..... Hwang Chii Ching

TITLE OF THESIS ..... Air Pollution Study within an Urban Valley

.....

DEGREE FOR WHICH THESIS WAS PRESENTED ..... M.Sc.

YEAR THIS DEGREE GRANTED 1978

Permission is hereby granted to THE UNIVERSITY OF ALBERTA LIBRARY to reproduce single copies of this thesis and to lend or sell such copies for private, scholarly or scientific research purposes only.

The author reserves other publication rights, and neither the thesis nor extensive extracts from it may be printed or otherwise reproduced without the author's written permission.

(Signed)

PERMANENT

#218 (

Town,

of Chi

DATE July 31 1978

THE UNIVERSITY OF ALBERTA

AIR POLLUTION STUDY WITHIN AN URBAN VALLEY

by

© HWANG CHII CHING

A THESIS

SUBMITTED TO THE FACULTY OF GRADUATE STUDIES AND RESEARCH

IN PARTIAL FULFILMENT OF THE REQUIREMENTS FOR THE DEGREE

OF MASTER OF SCIENCE

IN

METEOROLOGY

DEPARTMENT OF GEOGRAPHY

EDMONTON, ALBERTA

FALL, 1978

THE UNIVERSITY OF ALBERTA

FACULTY OF GRADUATE STUDIES AND RESEARCH

The undersigned certify that they have read, and recommend to the Faculty of Graduate Studies and Research, for acceptance, a thesis entitled Air Pollution Study within an Urban Valley submitted by Hwang Chii Ching in partial fulfilment of the requirements for the degree of Master of Science.

Date..July 31....1978

ABSTRACT

The problem of air pollution in valleys is reviewed and it is concluded that high concentrations of pollutants can result from inversion trapping, stagnation, impingement, downwash, and recirculation of air in valley wind systems. The special case of motor vehicle sources within a small urban river valley, involving some but not all of these processes, is the subject of this thesis. A field experiment that included simultaneous meteorological and carbon monoxide measurements in a cross-section of the North Saskatchewan River Valley in downtown Edmonton on July 20, 1977 is described. Carbon monoxide traverses revealed a fairly well-defined evening maximum concentration near the valley bottom and two peak concentrations in the vertical. The latter are attributed to incomplete vertical mixing of emissions from major bridges that cross the river nearly at two levels. A simple two-large box model is formulated for time changes in average pollutant concentrations in the valley. Predicted hourly mean carbon monoxide concentrations in the lower box are similar in magnitude to observed mean values. The model predicts an evening maximum in carbon monoxide concentrations because of decreasing vertical exchange and decreasing horizontal transport. The box model is easy to use and well suited for studying time changes. However, detailed measurements are needed in order to derive reliable spatial averages because of the large and complicated variations of temperature, wind, turbulence, and pollutant concentration within a valley.

ACKNOWLEDGEMENT

I am sincerely grateful to a number of people and organizations for their assistance and support in the preparation of this thesis.

First of all, I am deeply indebted to my departmental supervisor Dr. K. D. Hage for his patience, invaluable guidance, encouragement, and understanding throughout the period required for me to complete the thesis. Here, I would like to express my sincerest thanks to him for all his kind help.

Many thanks are owed to the Research Secretariat of Alberta Environment who provided financial support for my thesis research. Several Departments of the City of Edmonton provided some of the data required for this research work. In addition, many thanks go to Dr. E. R. Reinelt and Dr. D. J. Wilson for serving on my examining committee and providing invaluable advice.

I wish to express my sincere gratitude to Mr. Myron Oleskiw for his encouragement, assistance, and care during the time when I was studying in this country.

Finally, I would like to thank all Department Faculty members for their assistance and enthusiastic support during the time when I was in Canada.

TABLE OF CONTENTS

LIST OF TABLES

LIST OF FIGURES

FIGURE PAGE

LIST OF SYMBOLS

A: Area taken over the cross-valley plane. (m^2)

A_1: Area of the end face of Box 1 in the along-valley axis direction and is in the upstream side. (m^2)

A_2: Area of the end face of Box 1 in the along-valley axis direction and is in the downstream side. (m^2)

A_h: Area taken over the horizontal plane within the valley at height h. (m^2)

c: Pollutant concentration of Box 1. (ppm)

$\bar{c}$: Short-time mean-state pollutant concentration of Box 1. (ppm)

c_1,c_2: Short-time mean-state pollutant concentration measured over plane A_1 and A_2 respectively. (ppm)

C(t): Spatial-mean pollutant concentration obtained from CO-measurements. (ppm)

h: Height of Box 1. (m)

K_c: Turbulent diffusivity of pollutant mass. ($m^2.s^{-1}$)

K_h: Thermal turbulent diffusivity. ($m^2.s^{-1}$)

$K_c(h)$: Turbulent diffusivity of pollutant mass at height h. ($m^2.s^{-1}$)

L: Length of Box 1 in the along-valley direction. (m)

L': Open boundary length of Box 1 in the along-valley direction. (m)

M: Mass of pollutants. (gm)

Q_i: Pollutant source strength. ($ppm.s^{-1}$)

Q_l: Line pollutant source strength. ($ppm.m^{-1}.s^{-1}$)

$q(t)$: Time-dependent pollutant concentration of Box 1 which is obtained from taking the spatial mean of c. (ppm)

$q_t(t)$: Time-dependent pollutant concentration of Box 2 which is obtained from taking the spatial mean of c of Box 2. (ppm)

q_o: Initial pollutant concentration for the modelling calculation.

q^*: Quasi-equilibrium pollutant concentration. (ppm)

t': Dimensionless time.

$\bar{u},\bar{v},\bar{w}$: Wind velocity components in east-west, north-south, and vertical direction respectively (in Chapter III and Chapter IV) or in cross-valley, along-valley, and vertical direction respectively (in Chapter II). ($m.s^{-1}$)

$\bar{u}_1,\bar{v}_1$: Wind velocity component measured over A_1. ($m.s^{-1}$)

$\bar{u}_2,\bar{v}_2$: Wind velocity component measured over A_2. ($m.s^{-1}$)

$\bar{u}_b,\bar{v}_b$: Mean wind speed in the east-west and north-south direction respectively, averaged over the height of Box 1. ($m.s^{-1}$)

$\bar{V}_b$: $u_b^2 \quad v_b^2$. ($m.s^{-1}$)

$\bar{u}_B$: Mean wind speed component in the along-valley direction. ($m.s^{-1}$)

$\bar{v}_B$: Mean wind speed component in the cross-valley direction. ($m.s^{-1}$)

u^*: Frictional velocity. ($m.s^{-1}$)

R_i: Richardson number

ζ: Dimensionless height. (m)

ϕ_v: Dimensionless wind shear.

ϕ_h: Dimensionless temperature gradient.

U^*: Bulk value of wind speed. ($m.s^{-1}$)

T^*: Vertical turbulent flushing frequency. (s^{-1})

T: Temperature. (^{o}C)

T_1: Temperature measured at height z_1. (^{o}C)

T_2: Temperature measured at height z_2. (^{o}C)

θ: Potential temperature. (^{o}K)

γ_d: Dry adiabatic lapse rate. ($^{o}C.m^{-1}$)

γ: Lapse rate. ($^{o}C.m^{-1}$)

CHAPTER I

INTRODUCTION

1.1 The problem

A simple definition of air pollution is the contamination of air around us caused by the release of waste materials into the atmosphere. A more rigorous definition given by the Engineering Joint Council of the U.S.A. is '' the presence in the outdoor atmosphere of one or more contaminants, such as dust, fumes, gas, mist, odour, smoke, or vapor, in quantities, of characteristics, and duration, such as to be injurious to human, plant, or animal life, or to property, or to interfere unreasonably with the comfortable enjoyment to life and property.'' (1964). Examples of release of waste materials which cause air pollution are the exhaust from automobiles, generation of energy, industry, etc..

The atmosphere can transport pollutants from the pollutant sources to receptors and dilute the pollutant concentration. The tendency of pollutants to diffuse across the mean wind varies greatly. Empirical and theoretical studies show that the diffusive power of the atmosphere depends on the wind speed, surface roughness, and thermal stability of the atmosphere.

Industries, resort and housing developments, and associated transportation systems are often found in low terrain, e.g., along rivers, in valleys, at the base of mountains, or by a lake or ocean

shore. Therefore, the problem of how well pollutants will diffuse under constraints imposed by terrain features is an important issue. In the present study, we are concerned only with an urban river valley. The valley acts as a physical barrier which prevents the lateral or cross-valley diffusion which normally occurs over level country. If an inversion forms the possibility exists for accumulation of pollutants within the valley because of poor ventilation. In addition, it seems possible that such a valley inversion may be enhanced in an urban setting because of the heat-island effect which lead to advection of warm air above the valley at night. Panofsky (1968) stated that the conditions for particularly severe air pollution are: (1) light wind or calm, (2) very small mixing depth, (3) poor ventilation, (4) a region with frequent anticyclones, (5) a mountain, or hill, or valley region. If these conditions happen simultaneously they can lead to disastrous consequences. Egan (1975) showed that in sheltered regions under some kinds of weather conditions poor ventilation occurs with disastrous consequences in the form of air pollution episodes. A well-known example of this kind of episode happened in the Meuse River Valley in Belgium in 1930. The Meuse River Valley is narrow in shape, 1 km between ridge line, 24 km in length, and with hills about 90 m high on either side. A large number of industrial plants were located in the valley. From Firket's report (1936), severe pollution occured there during the period December 1 to 5, 1930. It was reported that anticyclonic conditions prevailed during that period. An

inversion confined the pollutants within the valley and fog, along with very light winds, occurred at that time to carry pollutants from the city of Liege and from industrial plants nearby into a narrow portion of the valley. In the original report on the episode, it was estimated that the SO_2 content of the atmosphere ranged from 9.6 ppm to 38.4 ppm. These conditions were favourable for particularly severe air pollution. It is assumed that oxidation of the SO_2 results in high sulfuric acid mist concentrations. When SO_2, dissolved or otherwise, combined with water droplets in the presence of a multiplicity of other pollutants it was oxidized to sulfuric acid mist forming particles sufficiently small to penetrate deeply into the lung. As a result several hundred people suffered from acute respiratory troubles, and sixty three died on December 4 and 5. A similar disaster occurred at Donora, Pa., during the period October 27 to 31, 1948. Donora is located in a relatively deep and narrow valley of the Monongahela River at a distance of about 32km from Pittsburgh. During the five-day period of light winds associated with anticyclonic conditions, the pollution became severe and twenty persons died and hundreds were stricken in and near Donora. The episode of 1948 in Donora was not unique. A sequence of meteorological circumstances from October 4 to 14 in 1923 also led to serious smog conditions in the vicinity of Donora. Because of such evidence of lethal pollutant concentrations in the valley communities, there is an urgent need for both theoretical and observational programs of study of air pollution

within valleys. Hewson (1951) suggested that, given a knowledge of certain meteorological quantities in and just above a valley, of the rate at which pollutants are released into the valley, and of the topography of the valley, we can then compute the rate of accumulation of impurities in a given section of a valley during prolonged stagnant atmospheric conditions.

The proposed research is believed to be important, because the North Saskatchewan River in Edmonton passes through almost all core portions of the city. The objectives of this investigation are to carry out a pilot modelling study for the North Saskatchewan River Valley in Edmonton and experimental studies of air quality in relation to possible urban heat-island enhancement of valley inversions and to organized valley wind systems.

1.2 Valley microclimatology and air pollution

1.2.1 General reviews

Pasquill (1968) showed that the geometry of the surface over which the air stream passes can cause a deflection of the air stream, or modify the rate of mixing and consequent dilution of the materials carried with it. Egan (1975) showed that impingement from elevated pollutant sources on hill or mountain sides may result in high ground level pollutant concentration. Valley microclimate has been studied for a long time. Munn (1966) and Yoshino (1975) presented detailed reviews of this problem. Summarizing their results, we conclude that valley microclimate depends on (1) the geometrical dimensions of the valley, including length, width, depth, slope of the sides, slope of the valley floor, and presence of bends or constrictions, (2) the orientation of the valley, (3) the prevailing wind direction, (4) the properties of the earth's surface, and (5) the variation of solar radiation with different seasons. A complete discussion of valley microclimate embracing the solar radiation balance, air temperature, ground temperature, wind, precipitation, evaporation, fog, and phenology is contained in Yoshino (1975). For the present study, we are concerned primarily with knowledge of the circulation and temperature distribution of the air within a valley. Although all of these climatic elements are correlated with one another, the valley air circulation and valley thermal stability determine the advective transport and turbulent transport of pollutants. Therefore, we only consider these two factors

in the present study.

1.2.2 Wind and temperature in the valley

1.2.2.1 Wind

Mountain-valley regions have their own local circulation patterns. During the nighttime, the air above the valley sides is cooled and sinks to the lower portion of the valley. Because the valley itself forms a slope, as shown by the flow of the water in the river, the denser air from the valley sides flows downstream under the influence of gravity. During the daytime the valley sides are heated by insolation, the air rises along the valley sides and there is a flow of air upstream along the valley axis. Defant (1949) has summarized the basic theory and observations of mountain-valley local circulation system caused by the combination of diurnal surface-heating and -cooling cycles and sloping surfaces, and he presented a famous schematic illustration for the diurnal variation of circulation systems of the valley reproduced here in Fig. 1.1 Defant's model was derived assuming no prevailing upper wind, and neglecting possible effects due to orientation of the valley slopes. Actually, mountain- and valley- breezes vary according to topographical conditions, seasonal change of the position of the sun, earth's surface conditions, prevailing upper level wind, etc.. Hewson and Longley (1944) described the results of observations at Columbia Garden near the center of the Columbia River Valley in Southern British Columbia, near the city of Trail. The experimental results show that the regularity of the down-valley motion at night and the up-valley

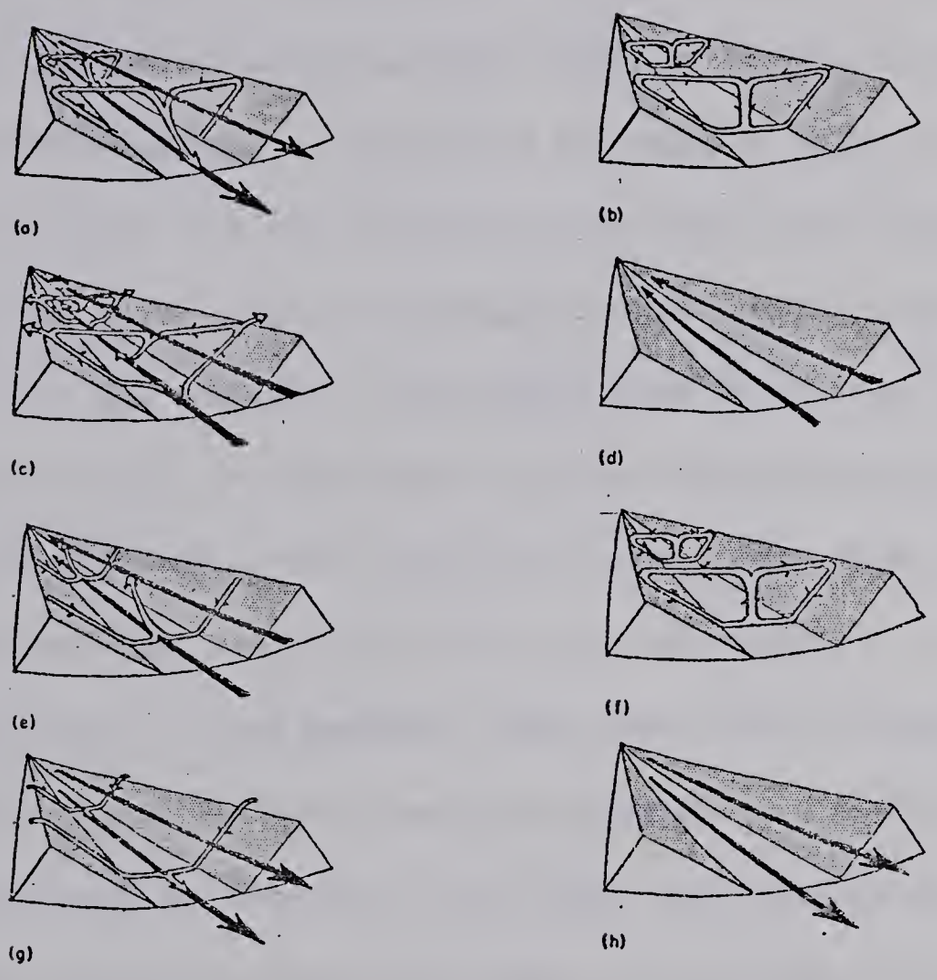

Fig. 1.1 Schematic illustration of the normal diurnal variations of the air currents in a valley. (After Defant (1949))
(a) Sunrise; onset of upslope winds (white arrows), continuation of mountain wind (black arrows). Valley cold, plains warm.
(b) Forenoon (about 0900); strong slope winds, transition from mountain wind to valley wind. Valley temperature same as plains.
(c) Noon and early afternoon; diminishing slope winds, fully developed valley wind. Valley warmer than plains.
(d) Late afternoon; slope winds have ceased, valley wind continues. Valley continues warmer than plains.
(e) Evening; onset of downslope winds, diminishing valley wind. Valley only slightly warmer than plains.
(f) Early night; well-developed downslope winds, transition from valley wind to mountain wind. Valley and plains at same temperature.
(g) Middle of night; downslope winds continue, mountain wind fully developed. Valley colder than plains.
(h) Late night to morning; downslope winds have ceased, mountain wind fills valley. Valley colder than plains.

motion in the daytime is striking, and the strength, as well as the regularity, of down-slope and up-slope flows varies with the locality. Davidson (1961) studied valley-wind phenomena in relation to air pollution problems. The data presented in his report were obtained from the local wind study program mentioned above and another program carried out at a site near Peekskill in the Hudson River Valley from 1955 to 1957. In the report, he showed that (1) when the prevailing upper level wind is strong enough it will destroy the valley wind system, (2) when the prevailing wind is weak, the wind type in the valley is a valley-slope wind. Fig. 1.2 from Davidson (1961) showed that the turbulence experienced in a valley varies markly with location in the valley, and with the strength and direction of the upper level prevailing flow. Of particular interest for the present study is the micrometeorological study of the North Saskatchewan River Valley in Edmonton by Klassen (1962). He showed that if the prevailing upper level wind reaches some value, it will penetrate the valley and predominate to the valley floor. He also speculated that slope winds in the valley drained down to the river edge at night and then rose to form a two-cell circulation because of the heat source provided by river water. Munn (1966) summarized the air flow in a valley as follows: (1) When a strong prevailing upper-level wind is blowing in a direction more or less parallel to the valley, a funnelling effect may occur. (2) When a strong prevailing wind is blowing at right angles to the valley, wind speed in the valley is less than that over level country, and there are regions of intense turbulence

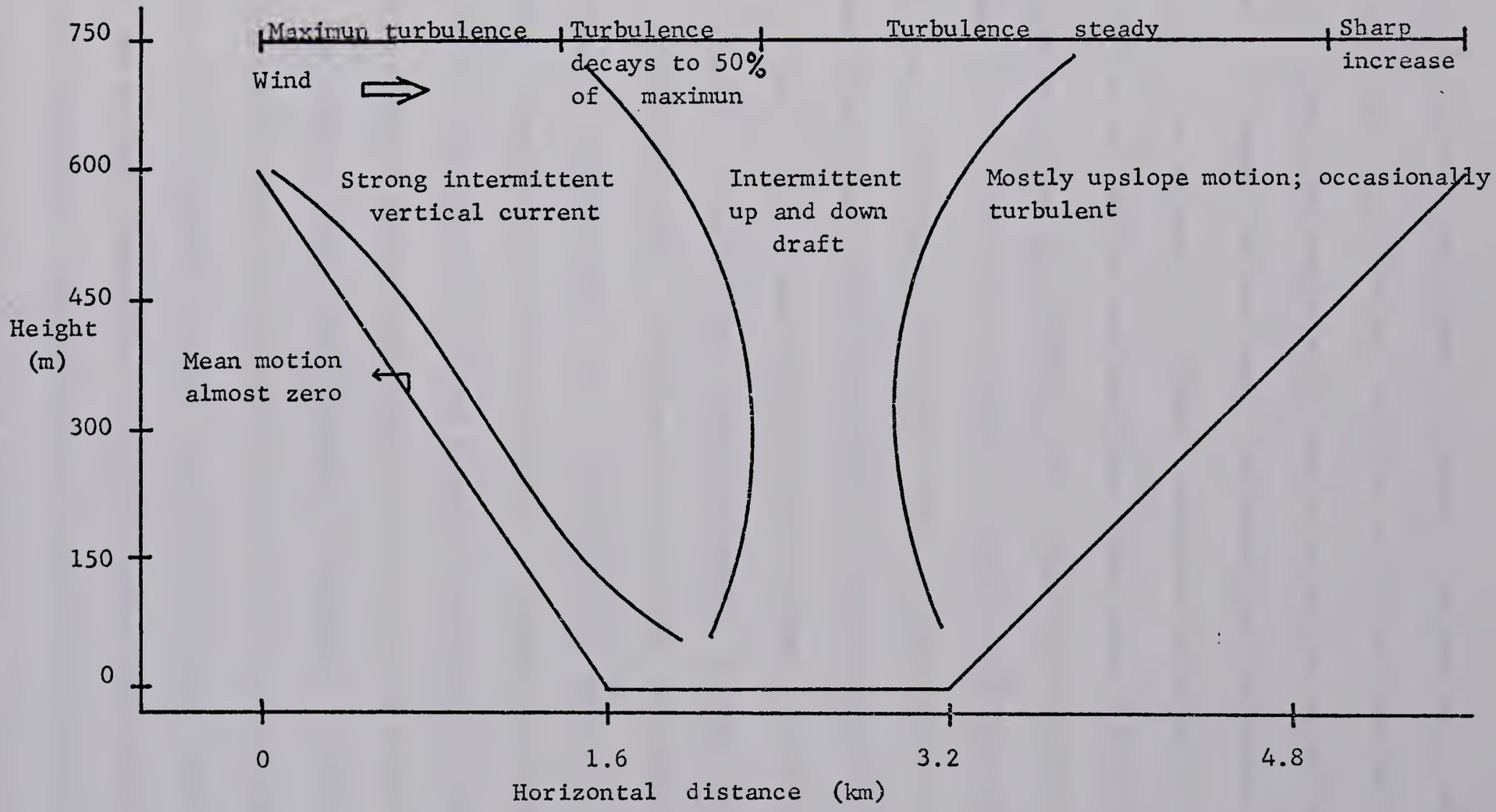

Fig. 1.2 Schematic sketch of distribution of vertical currents and turbulence with prevailing flow normal to ridge line . (From Davidson (1961))

as shown in Fig. 1.2 . (3) When the prevailing upper-level wind is weak, the valley wind and slope wind may develop fully. In addition, he concluded that water bodies and minor topographical features may affect the local wind system in the valley. Table 1.1 and Fig. 1.3 from Stern, et al (1973) show the net results of several principles operating in mountain-valley topography on the mesoscale. First, an east-west trending valley has only one sunny slope with heated up-slope during the daytime. A north-south trending valley has slopes about equally heated during the high sun hours of greatest heating. Second, windflow parallel to a ridge line will scour a land scape without a tendency to form separated flow such as is encountered in flow perpendicular to a ridge line. Finally, thermally-produced circulations on slopes (up-slope with heating, and downslope with cooling) combine with mechanically-produced circulations such as eddies and helices. Three points emphasized by Stern, et al (1973) are that : (1) vigorous mesoscale circulations may supress the features shown in Table 1.1 and Fig.1.3 , (2) under some circumstances one flow pattern may alternate with another during the course of several hours under conditions when neither one has both thermal and mechanical components strongly reinforcing each other, (3) variable macroscale wind speeds and directions may change the location of the separation surface up or down slope unless the presence of a salient edge tends to fix its location. The result for a particular site on an upper slope may be a reversal of wind direction as the surface

Table 1.1 Generalized mesoscale windflow pattern associated with different combinations of wind direction and ridge line orientation. (From Stern, et al (1973))

Wind direction relative to ridge line	Time of day	Ridge line orientation	
		East-west	North-south
Parallel	Day	South facing slope is heated - single helix	Upslope flow on both heated slope - double helix
	Night	Downslope flow on both slope - double helix	Downslope flow on both slope - double helix
perpendicular	Day	South facing slope is heated north wind - stationary eddy fills valley south wind - eddy suppressed flow without separation	Upslope flow on both heated slope - stationary eddy one half of the valley
	Night	Indefinite flow extreme stagnation in valley bottom	Indefinite flow extreme stagnation in valley bottom

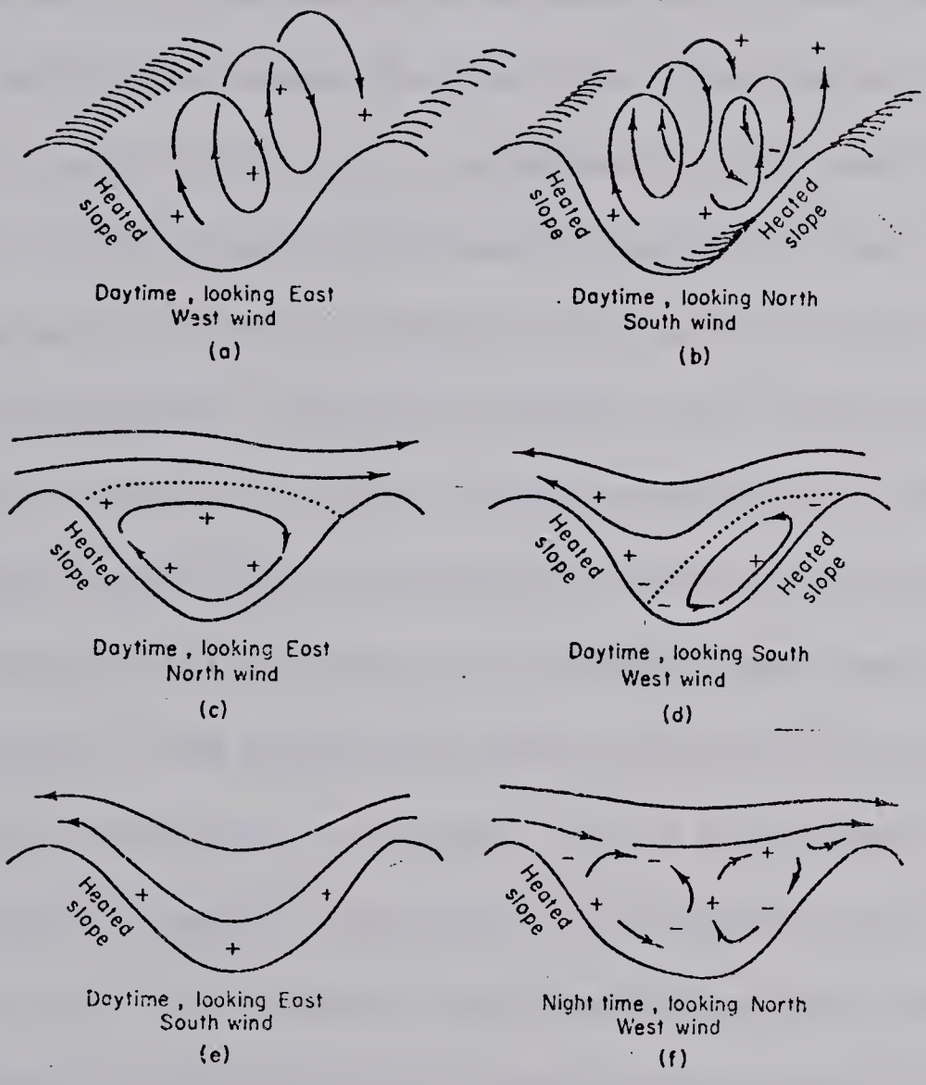

Fig. 1.3 Mesoscale flow patterns described in Table 1.1. Reinforcement of thermal and mechanical circulations is marked + ; opposition, - . (From Stern, et al (1973))

moves across the site.

Davidson (1961) cautioned that valleys differ enormously with respect to the height of the walls, the slope of walls, the direction of the valley, the distance between the ridge lines, the slope of the valley floor, and the length of the valley. He indicated at the time of writing that a general theory of valley winds was not available. Indeed, the situation remains so at present especially when we try to take into account the valley surface conditions, latitude of the valley, and man-made construction within the valley or along the valley rim. Yoshino (1975) discussed several kinds of valley microclimates such as those associated with very shallow valleys, small valleys, very large valleys, V-shape valleys, etc.. He admitted that there are many variations of mountain-valley circulations. For example, where a valley leads to a plain from a mountain range a strong local wind sometimes occurs. In small valleys there is an obvious interaction between the prevailing upper level wind and the valley wind. In very shallow valleys the valley winds are often subdued by gradient winds whereas mountain winds may be quite well developed, etc.. For more detail the reader is referred to the textbooks by Munn (1966) and Yoshino (1975).

1.2.3 Air pollution in the valley

When a strong prevailing wind is blowing over the plain above the valley in a direction at right angles to the valley orientation, the wind speed in the valley is usually smaller than that over the plain. Scorer (1959) showed that there is an aerodynamic downwash along the slopes of the valley under favourable condition such as with wind speeds above some threshold value. This could result in high ground-level pollutant concentrations from elevated pollutant sources on the plain. On the other hand, in light prevailing winds, the preferred wind patterns within the valley are frequently dominated by up-valley or down-valley flow. Hence, in the valley over long time periods the pollutant concentration from valley sources may be higher than that in the plain above.

Valleys are favourable locations for inversions. The intensity of the inversion is often not great because of the continual overturning of air. Usually, the nighttime turbulence levels in the valleys are higher than those over the plains above. Accordingly, mixing may be appreciable within the valley at night even though an inversion exists. If an urban heat-island exists along the plains above the valley such as could happen in Edmonton this may enhance the nighttime valley inversion by the advection of relative warm air from the city on all sides. As a result, the vertical exchange between valley air and urban air above may be suppressed. From the above discussion, as well as from a general

consideration of the sheltering effect of the valley, it seems possible that poor ventilation and accumulation of pollutants from local sources could happen at times in the urban valley site under study.

CHAPTER II

MODELLING STUDY OF AIR POLLUTION WITHIN THE VALLEY

2.1 Introduction

An air pollution prediction model will be developed in this Chapter for application to the prediction of air pollution concentrations within the valley region. The investigation begins with the development of a simple box model for time variations in pollutant concentration. There are two boxes in the model; in general, one is in the river valley and the second is in the city atmosphere above. In some applications one box contains the air within the surface temperature inversion layer which is located in the lower portions of the valley during the nighttime hours and the second box is just above it. The box model is based on the conservation of pollutant mass and the conservation of air. Molecular diffusion, the turbulent fluxes in the horizontal direction, and the transport by mean vertical motion will not be considered, because they are assumed to be small in comparison with vertical turbulent fluxes and transport by the mean horizontal wind component. In valleys, the motion of air is assumed to be dominated by the along-valley wind component so that horizontal transport occurs mostly in the along-valley dimension. However, if there is an open boundary existing in the valley wall somewhere we have to consider the advective transport of pollutants

by the wind speed component in the cross-valley direction. In order to calculate the mean vertical transport of pollutants by turbulent flux, at the very least we need to know the bulk value of pollutant concentration in each of the two boxes. The detailed discussion of these simulations will appear in Chapter IV. In addition, we must estimate the turbulent diffusivity of pollutant transport and choose appropriate vertical distances for estimating the vertical pollutant concentration gradient between the two boxes. In order to calculate the mean transport by horizontal air motion, at the very least we need to know the spatial distribution of pollutant concentration over two cross-valley sections. However some modifications are needed in the present application because of equipment and fund limitations. These modifications will be discussed thoroughly in Chapter IV. Short-period time averages and space averages are used to find the bulk value of pollutant concentration as a time-dependent function.

Following Lettau (1970) the model equation is reduced to a simple form by the introduction of new variables such as the bulk value of horizontal wind speed and the flushing frequency. The bulk value of horizontal wind speed is a key variable in the process of horizontal advection. The flushing frequency is a measure of the time dependence of the bulk value of pollutant concentration.

The last part of this Chapter concerns the solution to the governing equation of the model. A more detailed discussion of the method

of solution to the governing equation for practical application to our study region, and some numerical calculation results are presented in Chapter IV.

2.2 The model

The two boxes of the model are labeled 1 and 2 in Fig. 2.1(a). Box 1 contains the river valley air and Box 2 contains the urban air. It can be seen in Fig. 2.1(b) that Box 1 is assumed to have a height h and a constant length L. The width of Box 1 is expressed by a function

$$W(x,z) = y_2(x,z) - y_1(x,z)$$

The coordinates, as indicated in Fig. 2.1(b) are chosen such that x is along the valley, y is across the valley, and z is in the vertical direction. Box 1 is defined as follows:

1. The bottom of Box 1 is the plane EFGH as shown in Fig. 2.1(b). This plane is coincident with the water surface of the river, ie. , with the plane $z = 0$. It is bounded by the planes $x = 0$ and $x = L$ and curves $y = y_1(x,0)$ and $y = y_2(x,0)$ where $x = \left\{ x \mid x \in [0,L] \right\}$.

2. The top of Box 1 is the plane ABCD as shown in Fig. 2.1(b). This plane is assumed to be parallel to EFGH and is at $z = h$. Curve AC and curve BD are along the rim of the valley sides. This plane is bounded by the lines $x = 0$ and $x = L$, and by the curves $y = y_1(x,h)$ and $y = y_2(x,h)$ where $x = \left\{ x \quad x \in [0,L] \right\}$.

3. The sides of Box 1 are ABCD, CDGH, ACEG, and BDGH. ACEG is a curved-surface which is coincident with the valley side. Mathematically, this

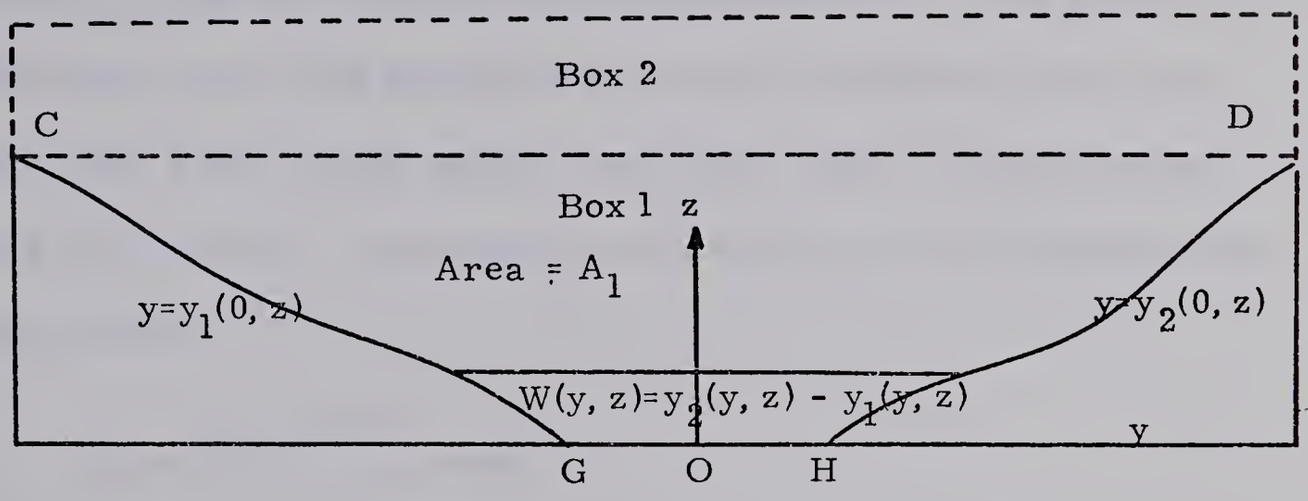

(a)

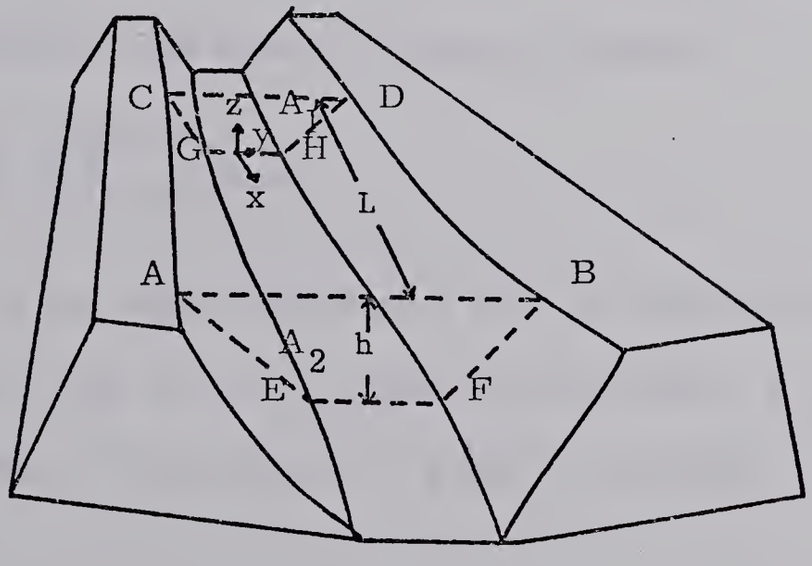

(b)

Fig. 2.1 Schematic diagrams show the relative positions of boxes in our Box model where (a) shows the cross-valley 2-dimensional view and (b) shows the 3-dimensional view.

plane can be expressed as $y = y_2(x,z)$ where $(x,z) = \{(x,z) \mid x \in [0,L], z \in [0,h]\}$. ABEF is a vertical cross-valley plane, i.e., the plane $x = L$. This plane contains the High Level Bridge and is bounded by the planes $z = 0$ and $z = h$, and by curves $y = y_1(L,z)$ and $y = y_2(L,z)$ where $z = \{z \mid z \in [0,h]\}$. The measure of this plane A_2 is given by the following equation:

$$A_2 = \int_0^h \int_{y_1(L,z)}^{y_2(L,z)} dy\, dz$$

CDGH is another vertical cross-valley plane, i.e., the plane $x = 0$. This plane is assumed to parallel to ABEF and is bounded by the curves $y = y_2(0,z)$ and $y = y_1(0,z)$ where $z = \{z \mid z \in [0,h]\}$. The measure of this plane A_1 can be found from the following equation

$$A_1 = \int_0^h \int_{y_1(0,z)}^{y_2(0,z)} dy\, dz$$

To sum up the above discussion, Box 1 is bounded by the four planes $x = 0$, L and $z = 0$, h, and by the surfaces $y = y_1(x,z)$ and $y = y_2(x,z)$ where $(x,z) = \{(x,z) \; x \in [0,L], z \in [0,h]\}$.

2.3 Averages and fluctuations

In order to derive the mean-state equation, it is necessary to take time- and space-averages following the Reynold's averaging procedure. The averaging operations filter out the fluctuations on all scales smaller than the scale defined by the time and space intervals over which the mean values are taken. If the averaging interval is large enough to include many oscillations, the averages of the fluctuations over this interval vanish by definition. Reynold's averages as used here are of two kinds; one is a time average and the second is a space average. In our study, we always express a physical variable as a sum of a mean-state part and a fluctuating part, i.e., we define

$$A = \bar{A} + A' \tag{2.1.1}$$

$$A = [A] + A'' \tag{2.1.2}$$

where A is the instantaneous value, $\bar{A}$ is the time-mean value, $[A]$ is the space-mean value, A' is the fluctuation of A with respect to $\bar{A}$, and A'' is the fluctuation of A with respect to $[A]$.

Mieghem (1973) has presented a very comprehensive discussion of the averaging problem. He showed that:

$$\overline{aA + bB} = a\bar{A} + b\bar{B} \text{ , or } [aA + bB] = a[A] + b[B] \tag{2.2.1}$$

$$\overline{\bar{A}\, B} = \bar{A}\,\bar{B} \text{ , or } [[A]\, B] = [A]\,[B] \tag{2.2.2}$$

$$\overline{\bar{A}} = \bar{A} \text{ , or } [[A]] = [A] \tag{2.2.3}$$

$$\overline{\bar{A}\,\bar{B}} = \bar{A}\,\bar{B} \text{ , or } [[A]\,[B]] = [A][B] \tag{2.2.4}$$

$$\overline{\frac{\partial A}{\partial s}} = \frac{\partial \bar{A}}{\partial s} \quad , \text{ or } \quad \left[\frac{\partial A}{\partial s}\right] = \frac{\partial [A]}{\partial s} \tag{2.2.5}$$

$$\overline{\bar{A}\, B'} = 0 \quad , \text{ or } \quad \left[[A]\, B''\right] = 0 \tag{2.2.6}$$

$$\overline{A\, B} = \bar{A}\,\bar{B} + \overline{A'B'} \quad , \text{ or } \quad [A\, B] = [A][B] + [A''B''] \tag{2.2.7}$$

where A and B are functions of spatial coordinates (x,y,z) and time t, a and b are constants, and s represents any coordinate (x,y,z,t).

Most pollutant concentration observations must be averaged over some time interval because instantaneous values are extremely variable. The model variables must be averaged over the same time period. A function f may be averaged over a time interval T centered at time t as follows:

$$\bar{f} = \frac{1}{T}\int_{t-\frac{T}{2}}^{t+\frac{T}{2}} f\, dt \tag{2.3}$$

The nature of the model for atmospheric pollution problems is such that we are only concerned with averages over a particular box having volume measure V. Let the space average of the representative function f be expressed as follows:

$$[\bar{f}] = \frac{1}{V}\iiint_V \bar{f}\, dxdydz \tag{2.4}$$

The space average of $\bar{f}$, i.e., $[\bar{f}]$ is a function of time only. Again, as discussed in connection with average, we can express the representative functions of our model as $\bar{f} = [\bar{f}] + f''$ and substitute this into the time-mean state equation. When the time-mean state equations of the model are averaged in accordance with (2.4), we obtain the final

governing equation of the model.

2.4 The governing equation for the box model

2.4.1 Some assumptions

A derivation of the governing equation for the box model is presented in this section. The following assumptions are needed

1. Horizontal turbulent fluxes are neglected because they are assumed to be small in comparison with horizontal advective transport by the mean wind.

2. The advective transport of pollutant is dominated by the along-valley wind component only, because the valley walls act as a barrier to prevent significant transport of pollutants from Box 1 in the cross-valley direction, i.e., let $\frac{\partial \bar{c}\bar{v}}{\partial y} = 0$. However the advection of pollutants in this direction must be included when we have an open boundary in some section of the valley walls.

3. The vertical advection of pollutants is too small to be counted in our calculation, i.e., let $\frac{\partial \bar{c}\ \bar{w}}{\partial z}=0$.

4. The mass of pollutants $M(x,y,z,t)$ within the valley is considered to be conservative, i.e., no deposition and chemical reaction of pollutants occur. Thus, the total rate of change of pollutant mass should be equal to the total rate of emission from pollutant sources. Mathematically, we can write this assumption as:

$$\frac{d\ M(x,y,z,t)}{d\ t} = \sum_{i=1}^{n} Q_i \qquad (2.5)$$

where M is mass of pollutants (gm), t is time (s), and Q_i^* is the emission rate of pollutants from the ith source ($gm.s^{-1}$, $i=1, 2,.., n$)

5. There are no area sources or point sources in Box 1. The only sources considered here are the line sources River Valley Road and the 105th Street Bridge.

---

* For point sources:

$$Q_i = Q_1 + Q_2 + \ldots\ldots\ldots\ldots\ldots\ldots + Q_n$$

where $Q_1, Q_2, \ldots\ldots, Q_n$ are point source emission rates ($gm.s^{-1}$).

For line sources:

$$Q_i = Q_{L_1} + Q_{L_2} + \ldots\ldots\ldots\ldots\ldots\ldots + Q_{L_n}$$

where Q_{L_i} are line source emission rates from ith source ($gm.s^{-1}.m^{-1}$, $i = 1, 2, 3, \ldots\ldots\ldots, n$).

For area sources:

$$Q_i = Q_{A_1} + Q_{A_2} + \ldots\ldots\ldots\ldots\ldots\ldots + Q_{A_n}$$

where Q_{A_i} are area sources emission rates ($gm.s^{-1}.m^{-2}$, $i = 1,2,\ldots\ldots,n$), and A_i are the measure of the area source (m^2, $i = 1, 2, 3, \ldots., n$).

2.4.2 Governing equation

The derivation of the model equations begins with the equation for conservation of pollutants within Box 1, i.e., $\frac{dM}{dt} = \sum_{i=1}^{n} Q_i$. Since $M = cV$ where c is the instantaneous pollutant concentration in Box 1 and V is the variable volume of Box 1 then (2.5) can be written as:

$$\frac{dc}{dt} + \frac{c}{V}\frac{dV}{dt} = \frac{\sum_{i=1}^{n} Q_i}{V} \qquad (2.6)$$

Expanding the total derivative, we have:

$$\frac{d(\ )}{dt} = \frac{\partial(\ )}{\partial t} + \vec{V} \cdot \nabla(\ )$$

where $\vec{V}$ is the velocity ($\vec{V} = u\,\vec{i} + v\,\vec{j} + w\,\vec{k}$). Substituting this equation into (2.6) we obtain:

$$\frac{\partial c}{\partial t} + \vec{V} \cdot \nabla c + \frac{c}{V}\frac{dV}{dt} = \frac{\sum_{i=1}^{n} Q_i}{V}$$

Furthermore $\frac{c}{V}\frac{dV}{dt} = c\,\frac{d\ln A}{dt}$ because $V = A.L$ and L is constant. The continuity equation for an incompressible fluid is given by $\nabla \cdot \vec{V} = 0$.

By definition of vector operations:

$$\vec{V} \cdot \nabla c + c(\nabla \cdot \vec{V}) = \nabla \cdot c\vec{V}$$

Therefore,

$$\frac{\partial c}{\partial t} + \nabla \cdot c\vec{V} + c\frac{d\ln A}{dt} = \frac{\sum_{i=1}^{n} Q_i}{V}$$

With reference to (2.1), we have:

$$c = \bar{c} + c'$$

$$\vec{V} = \bar{\vec{V}} + \vec{V}'$$

$$\ln A = \overline{\ln A} + (\ln A)'$$

where the overbar denotes time averages and the prime denotes the

fluctuating quantities.

Substituting the above expression into (2.7) and averaging (2.7) in accordance with (3.3) gives us the short-time mean-state equation:

$$\overline{\frac{\partial \bar{c}+c'}{\partial t}+\nabla.(\bar{c}+c')\,(\vec{\bar{V}}+\vec{V}')+(\bar{c}+c')\,(\frac{d\,\overline{\ln A}}{dt}+\frac{d(\ln A)'}{dt})}=\frac{\sum_{i=1}^{n}Q_i}{V}$$

According to the definition of the averaging operation discussed in Section 2.3:

$$\overline{\frac{\partial \bar{c}+c'}{\partial t}}+\overline{\nabla.(\bar{c}+c')\,(\vec{\bar{V}}+\vec{V}')}+\overline{(\bar{c}+c')\,(\frac{d\,\overline{\ln A}}{dt}+\frac{d(\ln A)'}{dt})}=\frac{\sum_{i=1}^{n}Q_i}{V}$$

In addition, we have the following results by definition:

$$\overline{\frac{\partial \bar{c}+c'}{\partial t}}=\frac{\partial\overline{\bar{c}+c'}}{\partial t}=\frac{\partial \bar{c}}{\partial t}$$

$$\overline{\nabla.(\bar{c}+c')(\vec{\bar{V}}+\vec{V}')}=\nabla.(\bar{c}\vec{\bar{V}})+\nabla.(\overline{c'\vec{V}'})$$

$$\overline{(\bar{c}+c')(\frac{d\,\overline{\ln A}}{dt}+\frac{d(\ln A)'}{dt})}=\bar{c}\,\frac{d\,\overline{\ln A}}{dt}+\overline{c'\frac{d(\ln A)'}{dt}}$$

We assume $\overline{c'\,\frac{d(\ln A)'}{dt}}=0$, because this quantity is very difficult to measure and its value is expected to be very small. Therefore,

$$\bar{c}\,\frac{d\,\overline{\ln A}}{dt}+\nabla.(\bar{c}.\vec{\bar{V}})+\nabla.(c'.\vec{V}')+\frac{\partial \bar{c}}{\partial t}=\frac{\sum_{i=1}^{n}\bar{Q}_i}{V}$$

Expanding this vector equation into scalar terms, the short-time mean-state equation becomes

$$\frac{\partial \bar{c}}{\partial t}+\left(\frac{\partial \bar{c}\,\bar{u}}{\partial x}+\frac{\partial \bar{c}\,\bar{v}}{\partial y}+\frac{\partial \bar{c}\,\bar{w}}{\partial z}\right)+\left(\frac{\partial\overline{c'u'}}{\partial x}+\frac{\partial\overline{c'v'}}{\partial y}+\frac{\partial\overline{c'w'}}{\partial z}\right)+\bar{c}\,\frac{d\,\overline{\ln A}}{dt}=\frac{\sum_{i=1}^{n}\bar{Q}_i}{V}\qquad(2.8)$$

Let us consider the simplest case and assume that the valley walls have no open boundaries. Assumptions 1, 2, and 3 in section 2.4.1 take the following mathematical form:

$$\frac{\partial \bar{c}\,\bar{u}}{\partial x} + \frac{\partial \overline{c'w'}}{\partial z} \gg \frac{\partial \bar{c}\,\bar{v}}{\partial y} + \frac{\partial \bar{c}\,\bar{w}}{\partial z} + \frac{\partial \overline{c'u'}}{\partial x} + \frac{\partial \overline{c'v'}}{\partial y}$$

With this assumption, (2.8) can be written as follows:

$$\frac{\partial \bar{c}}{\partial t} + \frac{\partial \bar{c}\,\bar{u}}{\partial x} + \frac{\partial \overline{c'w'}}{\partial z} + \bar{c}\frac{d\,\overline{\ln A}}{d\,t} = \frac{\sum_{i=1}^{n} \bar{Q}_i}{V} \qquad (2.9)$$

Again, averaging (2.9) in accordance with (2.3) results in the following governing equation of our model:

$$\left[\frac{\partial \bar{c}}{\partial t} + \frac{\partial \bar{c}\,\bar{u}}{\partial x} + \frac{\partial \overline{c'w'}}{\partial z} + \bar{c}\frac{d\,\overline{\ln A}}{d\,t}\right] = \left[\frac{\sum_{i=1}^{n} \bar{Q}_i}{V}\right]$$

As discussed in Section 2.3 the above equation can be transformed into the following form by the definition of the averaging operation:

$$\underset{A}{\left[\frac{\partial \bar{c}}{\partial t}\right]} + \underset{B}{\left[\frac{\partial \bar{c}\,\bar{u}}{\partial x}\right]} + \underset{C}{\left[\frac{\partial \overline{c'w'}}{\partial z}\right]} + \underset{D}{\left[\bar{c}\frac{d\,\overline{\ln A}}{d\,t}\right]} = \underset{E}{\frac{\left[\sum_{i=1}^{n} \bar{Q}_i\right]}{V}} \qquad (2.10)$$

Consider the individual terms in this equation.

1. Term A

The quantity $\bar{c}$ is a space- and time-dependent function. After taking the space average of $\bar{c}$ over Box 1, i.e. $[\bar{c}]$, then the function $[\bar{c}]$ depends on time only. By letting $[\bar{c}] = q(t)$, this term may be written:

$$\left[\frac{\partial \bar{c}}{\partial t}\right] = \frac{\partial [\bar{c}]}{\partial t} = \frac{d\,q(t)}{d\,t}$$

We call q(t) the bulk value of pollutant concentration within Box 1.

2. Term B

According to (2.4), this term is given by $\left[\frac{\partial \bar{c}\,\bar{u}}{\partial x}\right]=\frac{1}{V}\iiint_V \frac{\partial \bar{c}\,\bar{u}}{\partial x}\,dV$ Theoretically, $\frac{\partial \bar{c}\,\bar{u}}{\partial x}$ is continuous in V and V is bounded by a closed surface which is discussed in Section 2.3. Referring to Gauss's Theorem, the volume integral can be transformed into the surface integral as follows for Box 1:

$$\iiint_V \frac{\partial \bar{c}\,\bar{u}}{\partial x}\,dV=\oiint_S (\bar{c}\,\bar{u})\,\vec{i}\,.\,d\vec{S}$$

$$=\iint_{ABEF} (\bar{c}\,\bar{u})\,\vec{i}.\vec{i}\,dS + \iint_{CDGH} (\bar{c}\,\bar{u})\,\vec{i}.(-\vec{i})dS +$$

$$\iint_{ABCD} (\bar{c}\,\bar{u})\,\vec{i}.\vec{k}\,dS + \iint_{EFGH} (\bar{c}\,\bar{u})\,\vec{i}.(-\vec{k})dS +$$

$$\iint_{ACEG} (\bar{c}\,\bar{u})\,\vec{i}.\vec{n}\,dS + \iint_{BDFH} (\bar{c}\,\bar{u})\,\vec{i}.(-\vec{n})dS$$

From vector mathematics, we have $\vec{i}\cdot\vec{i}=1$, and $\vec{i}\cdot\vec{k}=0$. There is a boundary condition which states that on the rigid boundary $u=0$, $v=0$, $w=0$. Because ACEG and BEFH are the valley walls, on these boundaries $u=0$ by this boundary condition. Therfore, we obtain $(\bar{u}\,\bar{c})=0$ on ACEG, and $(\bar{u}\,\bar{c})=0$ on BDFH. The above expression may be simplified to:

$$\iiint_V \frac{\bar{c}\,\bar{u}}{x}\,dV = \iint_{ABEF} (\bar{c}\,\bar{u})\,dS - \iint_{CDGH} (\bar{c}\,\bar{u})\,dS$$

$$=\iint_{A_2} (\bar{c}_2\,\bar{u}_2)\,dA_2 - \iint_{A_1} (\bar{c}_1\,\bar{u}_1)\,dA_1$$

$$= A_2\,\frac{1}{A_2}\iint_{A_2} (\bar{c}_2\,\bar{u}_2)\,dA_2 - A_1\,\frac{1}{A_1}\iint_{A_1} (\bar{c}_1\,\bar{u}_1)\,dA_1$$

$$= A_2\left[\bar{c}_2\,\bar{u}_2\right]A_2 - A_1\left[\bar{c}_1\,\bar{u}_1\right]A_1 \qquad (2.11)$$

where A_2 is the measure of ABEF, A_1 is the measure of CDGH, $\left[\ \right]_{A_2}$ and $\left[\ \right]_{A_1}$ are the surface averaging operators, $\bar{c}_1$ and $\bar{c}_2$ are the pollutant concentration fields distributed on ABEF and CDGH, respectively, and $\bar{u}_1$ and $\bar{u}_2$ are the along -valley wind speed fields distributed on CDGH and ABEF, respectively. With reference to (2.2), we define

$$\bar{c}_2 = \left[\ \bar{c}_2\ \right]_{A_2} + (\bar{c}_2)''$$

$$\bar{u}_2 = \left[\ \bar{u}_2\ \right]_{A_2} + (\bar{u}_2)''$$

$$\bar{c}_1 = \left[\ \bar{c}_1\ \right]_{A_1} + (\bar{c}_1)''$$

$$\bar{u}_1 = \left[\ \bar{u}_1\ \right]_{A_1} + (\bar{u}_1)''$$

where $\left[\ \right]_{A1}$ and $\left[\ \right]_{A2}$ denote the space averages which are taken over the surfaces having measure A_1 and A_2, respectively, and $(\ )''$ denotes the fluctuation of the defined variable with respect to its mean value.

Substituting the preceding expressions into (2.11), referring to the averaging operation rules discussed in Section 2.3, and omitting the small horizontal turbulent fluxes results in the following equation:

$$\frac{\partial \bar{c}\ \bar{u}}{\partial x} = \frac{1}{V}\left\{A_2\ [c_2]_{A_2}\ [u_2]_{A_2} + A_1\ [c_1]_{A_1}\ [u_1]_{A_1}\right\}$$

This equation has vast advantages in relation to the experimental research work and numerical applications. For example, we can make measurements of the CO-concentration field and along-valley wind speed field over the two end faces of Box 1 in the along-valley direction,

then we can calculate the advection of pollutants in the along-valley direction. The physical meaning of (2.12) is obviously that $A_2\{[\bar{c}_2]_{A_2}[\bar{u}_2]_{A_2}\}$ and $A_1\{[\bar{c}_1]_{A_1}[\bar{u}_1]_{A_1}\}$ are the fluxes of pollutant entering and leaving Box 1 through faces ABEF and CDGH, respectively.

3. Term C

According (2.4), this term is given by $\frac{\partial \overline{c'w'}}{\partial z} = \frac{1}{V}\iiint_V \frac{\partial \overline{c'w'}}{\partial z} dV$. As discussed under term B, using Gauss's Theorem the volume integral $\iiint_V \frac{\partial \overline{c'w'}}{\partial z} dV$ may be transformed as follows:

$$\iiint_V \frac{\partial \overline{c'w'}}{\partial z} dV = \oiint_S (\overline{c'w'})\vec{k}.\, d\vec{S}$$

$$= \iint_{ABEF}(\overline{c'w'})\vec{k}.\vec{i}\, dS + \iint_{CDGH}(\overline{c'w'})\vec{k}.(-\vec{i})dS +$$

$$\iint_{ABCD}(\overline{c'w'})\vec{k}.\vec{k}\, dS + \iint_{EFGH}(\overline{c'w'})\vec{k}.(-\vec{k})dS +$$

$$\iint_{ACEG}(\overline{c'w'})\vec{k}.\vec{n}\, dS + \iint_{BDFH}(\overline{c'w'})\vec{k}.(-\vec{n})dS$$

Again, from vector mathematics we have $\vec{k}\cdot\vec{i} = 0$, and $\vec{k}\cdot\vec{k} = 1$. In addition, following Lettau's (1970) suggestion, the quantity $(\overline{c'w'})_{z=o}$ is assumed to be equal to the area pollutant source strength. The same arguments may be applied to the terms $(\overline{c'w'})_{ACEG}$ and $(\overline{c'w'})_{BDFH}$. Since we have assumed that there are no area sources in our box model, then $(\overline{c'w'})_{EFGH} = (\overline{c'w'})_{ACEG} = (\overline{c'w'})_{BDFH} = 0$. The above equation is

then simplified as follows:

$$\iiint_V \frac{\partial \overline{c'w'}}{\partial z}\, dV = \iint_{ABCD} (\overline{c'w'})\, dS$$

But $(\overline{c'w'})_{ABCD} = (\overline{c'w'})_{z=h}$

and, $\overline{c'w'} = -K_c(z)\frac{\partial \bar{c}}{\partial z}$

Therefore,

$$\iiint_V \frac{\partial \overline{c'w'}}{\partial z}\, dV = \iint_{ABCD} K_c(h) \frac{\partial \bar{c}}{\partial z}\Big|_h\, dS$$

where $K_c(h)$ is the turbulent diffusivity of pollutant mass at the height h. Panofsky (1964) suggested that

$$\frac{\partial F}{\partial z}\Big|_h = (z_1 . z_2)^{1/2} = \frac{F_2 - F_1}{(z_1 . z_2)^{1/2} . \ln(z_2/z_1)}$$

for a variable that is distributed approximately as the logarithm with height. Since in our experiment the vertical pollutant concentration distribution decreases linearly upward in Box 1 and increase linearly upward in Box 2, $\frac{\partial \bar{c}}{\partial z}$ can then be calculated by

$$\frac{\partial \bar{c}}{\partial z} = \frac{\bar{c}_2 - \bar{c}_1}{z_2 - z_1}$$

where $\bar{c}_1$ and $\bar{c}_2$ are pollutant concentrations at $z_1 = \frac{h}{2}$ and $z_2 = \frac{3h}{2}$, respectively. It is obvious that $\bar{c}_1$ is measured in Box 1 with height h and $\bar{c}_2$ is measured in Box 2 with height h. Thus, we obtain :

$$\iiint_V \frac{\partial c'w'}{\partial z}\, dV = \frac{-K_c(h)}{h} \iint_{ABCD} (\bar{c}_2 - \bar{c}_1).dS$$

$$= \frac{K_c(h).A_h}{h} \left\{ \left[\bar{c}_1\right]_{A_h} - \left[\bar{c}_2\right]_{A_h} \right\}$$

Therefore,

$$\left[\frac{\partial \overline{c'w'}}{\partial z}\right] = \frac{K_c(h)\cdot A_h}{h.V}\left\{\left[\bar{c}_1\right]_{A_h} - \left[\bar{c}_2\right]_{A_h}\right\}$$

where A_h is the measure of the plane ABCD, and $\left[\quad\right]_{A_h}$ is the averaging operator taken over the plane ABCD.

4. Term D

The same arguments can be used to transform this term as follows:

$$\left[\bar{c}\cdot \frac{d\ \overline{\ln A}}{d\ t}\right] = q(t)\cdot\left[\frac{d\ \overline{\ln A}}{d\ t}\right] \qquad (2.13)$$

This equation is obtained by decomposing $\bar{c}$ and $\frac{d\ \overline{\ln A}}{d\ t}$ into space mean-state terms and turbulent terms, and then applying the operation rule discussed in Section 2.3 and linearizing it. This term can be regarded as a measure of the fractional volume change rate.

5. Term E

The joint source strength function $\sum_{i=1}^{n} Q_i$ depends on x, y, z, and t. It is difficult to obtain the value of $\sum_{i=1}^{n} Q_i$, if we consider it to be a function of time and space. However, if we consider it as a function of time only Q_i should be measureable. Let us define

$$S(t) = \frac{\left[\sum_{i=1}^{n} Q_i\right]}{V} \qquad (2.14)$$

From this time-dependent joint source strength function, we can obtain the required joint pollutant source strength at any time by adding the pollutant release rates from each source. Summing all terms we obtain:

$$\frac{dq(t)}{dt} + \frac{1}{V}\left\{A_2\left[\bar{c}_2\right]_{A_2}\left[\bar{u}_2\right]_{A_2} + A_1\left[\bar{c}_1\right]_{A_1}\left[\bar{u}_1\right]_{A_1}\right\} + q(t)\left[\frac{d\ \ln A}{dt}\right] +$$

$$\frac{K_c(h)\cdot A_h}{h.V}\left\{\left[\bar{c}_1\right]_{A_h} - \left[\bar{c}_2\right]_{A_h}\right\} = S(t) \qquad (2.15)$$

This is the governing equation of our box model for Box 1. It simulates the time variation of pollutant concentration within Box 1. In order to make practical use of this equation, we were forced to make several additional assumptions and simplifications, and these will represent additional error of this model. These are discussed in detail in Chapter IV. Nevertheless, if the errors are within acceptable ranges this model equation may be useful for the analysis of field data. The analysis of the model errors is an important topic for study. However, such a study was not feasible for this thesis. In addition, it would be very useful to derive a model for spatial variations in pollutant concentration, perhaps along the line proposed by Tang(1974).

2.4.3 Solution of governing equation

The governing equation (2.15) may be simplified by introducing time-dependent functions such as those suggested by Lettau (1970). These functions are the bulk value of wind speed U*(t), the vertical turbulent flushing frequency T*(t), and the total flushing frequency f*(t). They are introduced and discussed below:

1. U*(t)

The bulk value of wind speed is a parameter indicating the degree of advection of pollutants into or out of Box 1. It is defined by the following equation:

$$U^*(t) = \frac{1}{q(t) \cdot V} \left\{ A_2 \left[\bar{c}_2 \right]_{A_2} \left[\bar{u}_2 \right]_{A_2} - A_1 \left[\bar{c}_1 \right]_{A_1} \left[\bar{u}_1 \right]_{A_1} \right\} \quad (2.16)$$

U*(t) is obtained by dividing the term representing the advection of pollutants by q(t). The physical meaning of U*(t) is that it is a measure of the advection speed of pollutant into or out of Box 1. It depends on wind speed and on pollutant concentration within Box 1. The reciprocal of U*(t) divided by the length L of Box 1 is the characteristic time for transport of pollutants out of Box 1 by advection after the pollutants are released from their sources.

2. T*(t)

The vertical turbulent flushing frequency can be interpreted in the same way as L/U*(t), i.e., 1/T*(t) represents the time in which pollutants will be transported out of Box 1 by vertical turbulent diffusion after

release from the sources. T*(t) is defined as follows:

$$T^*(t) = \frac{K_c(h) \cdot A_h}{q(t).V.L} \left\{ \left[\bar{c}_1 \right]_{A_h} - \left[\bar{c}_2 \right]_{A_h} \right\} \qquad (2.17)$$

It depends on the atmospheric stability, the pollutant concentration gradient between Box 1 and the box immediately above Box 1, and on the dimensions of Box 1.

3. f*(t)

We define f*(t) as follows :

$$f^*(t) = \frac{U^*(t)}{L} + T^*(t) + \frac{d \ln A}{d t} \qquad (2.18)$$

This parameter is called the total flushing frequency. The reciprocal of f*(t) is a measure of the residence time for pollutants in Box 1 after they are released from their sources.

In terms of the above parameters, the original governing equation can be written in the form:

$$\frac{d\, q(t)}{d\, t} + f^*(t) \cdot q(t) = S(t)$$

Following Lettau (1970) we define a new independent variable t' as follows:

$$dt' = f^*(t) \cdot dt$$

where t' is dimensionless time. In addition, we define a quasi-equilibrium value of pollutant concentration q* as follows:

$$q^* = \frac{S(t)}{f^*} \tag{2.19}$$

In terms of t' and q* the governing equation becomes:

$$\frac{d\,q(t)}{dt'} + q(t) = q^* \tag{2.20}$$

which is similar to that of Lettau (1970). According to his suggestion, (2.20) can be solved as an initial-value problem if q* is quasi-constant over short time periods t'. The solution is:

$$q(t) = e^{-t'} \cdot \left(q_o + \int_o^{t'} e^{t'} . q^* \, dt' \right) \tag{2.21}$$

or

$$q(t) = e^{-t'} . \left\{ q_o + q^* . (e^{t'} - 1) \right\} \tag{2.22}$$

where q_o is the initial value of pollutant concentration at time t = 0. He showed in this paper that even for a time-independent source strength S(t), the value q* is actually a variable, because q* is controlled by f* which is a factor that depends on changing weather condition.

CHAPTER III

INSTRUMENTATION AND DATA COLLECTION

3.1 Introduction

Simultaneous air quality and meteorological measurements were made over a cross-section of the North Saskatchewan River Valley near the High Level Bridge in Edmonton. The present study is primarily concerned with Experiment 2 which was carried out on July 20, 1977 between late afternoon and midnight. Experiment 1 was rejected for lack of useable carbon monoxide concentration data. A brief description of the instrumentation and data collection procedures is given in this Chapter. The experimental data are used to estimate certain initial conditions and boundary conditions for the simple box model which was discussed in Chapter II. The pollutant emission rates and topographical parameters were derived from data supplied by the City of Edmonton. Some processing of these data was necessary because the original data were not in a form best suited for use in the model.

3.2 General characteristics of the site

The site chosen for the investigation was a cross-section of the North Saskatchewan River Valley between the High Level Bridge and the 105 th Street Bridge in Edmonton, Alberta. Edmonton is situated at $53^{o}33'N$ and $113^{o}35'W$ at an elevation of about 676 m above mean sea level on a sloping plateau. The section of this valley, where the

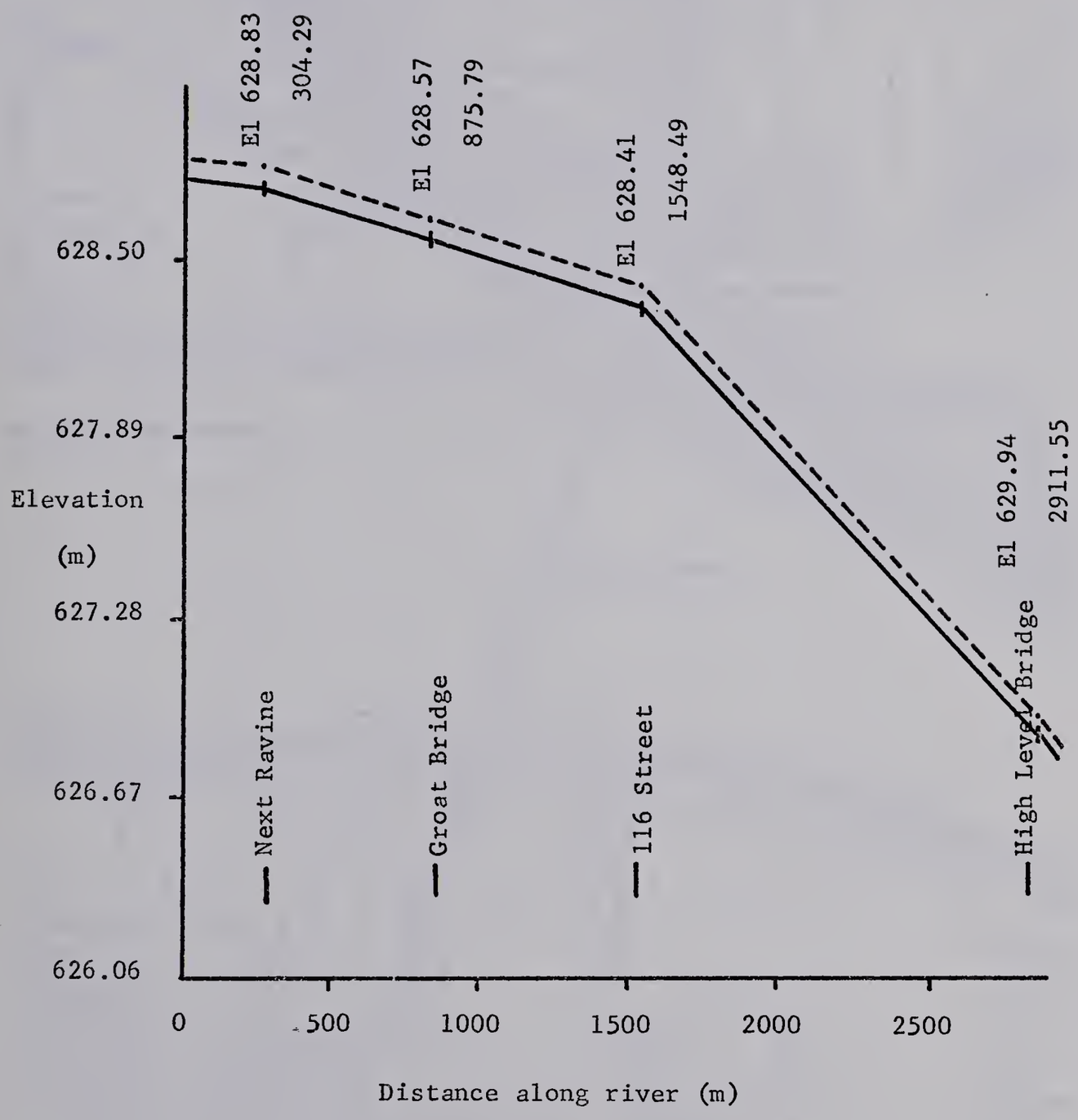

Fig 3.1 Profile of the North Saskatchewan River Valley between High Level Bridge and Mckinnon Ravine. The solid line represents water level and the dashed line represents ice level. (Source: City of Edmonton, Engineering Department based on measurements for February 20, 1961).

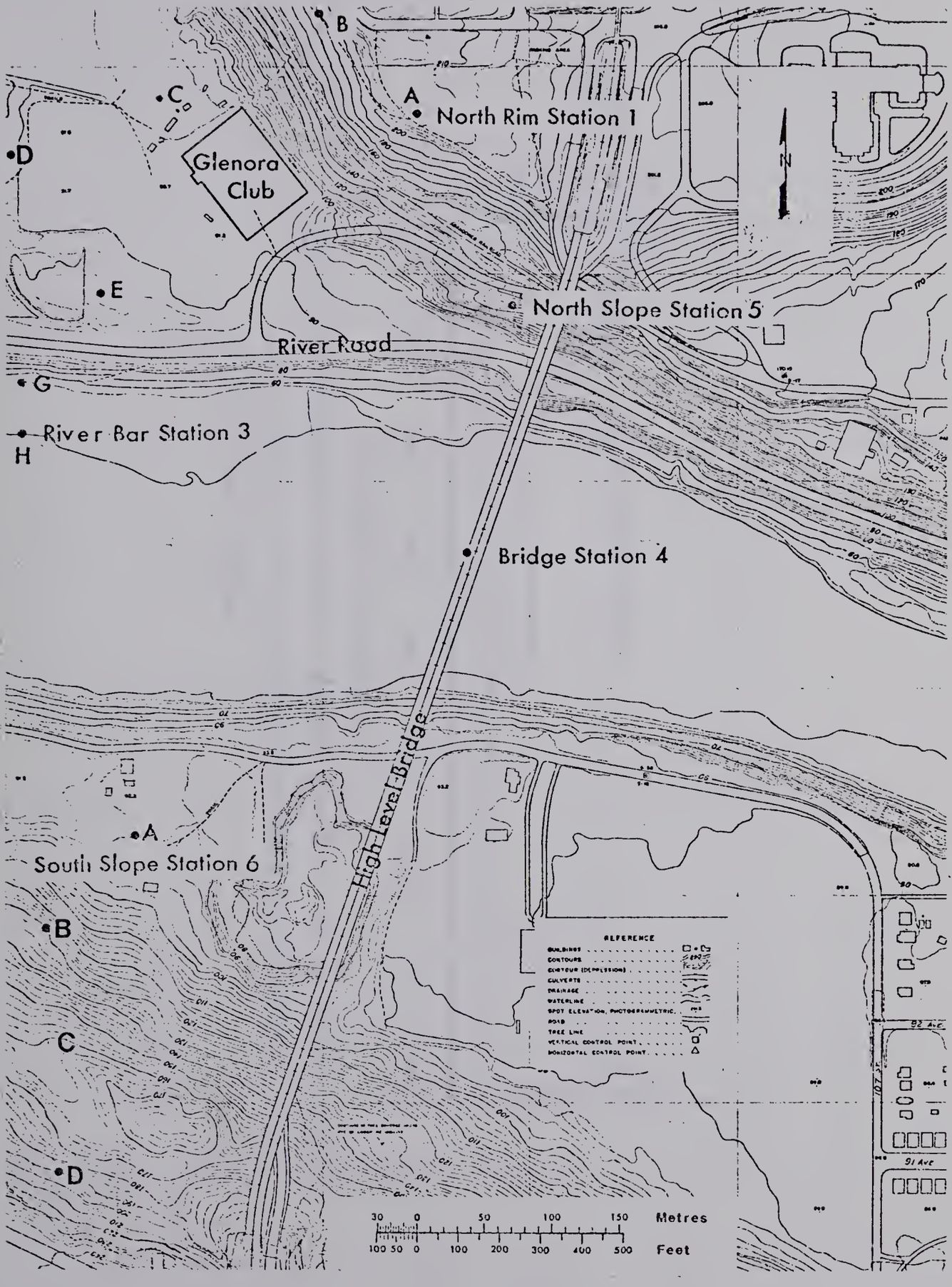

Fig. 3.2 A schematic showing the arrangements of experimental siting and the topographical feature of the investigated area. (Source: City of Edmonton, Engineering Department)

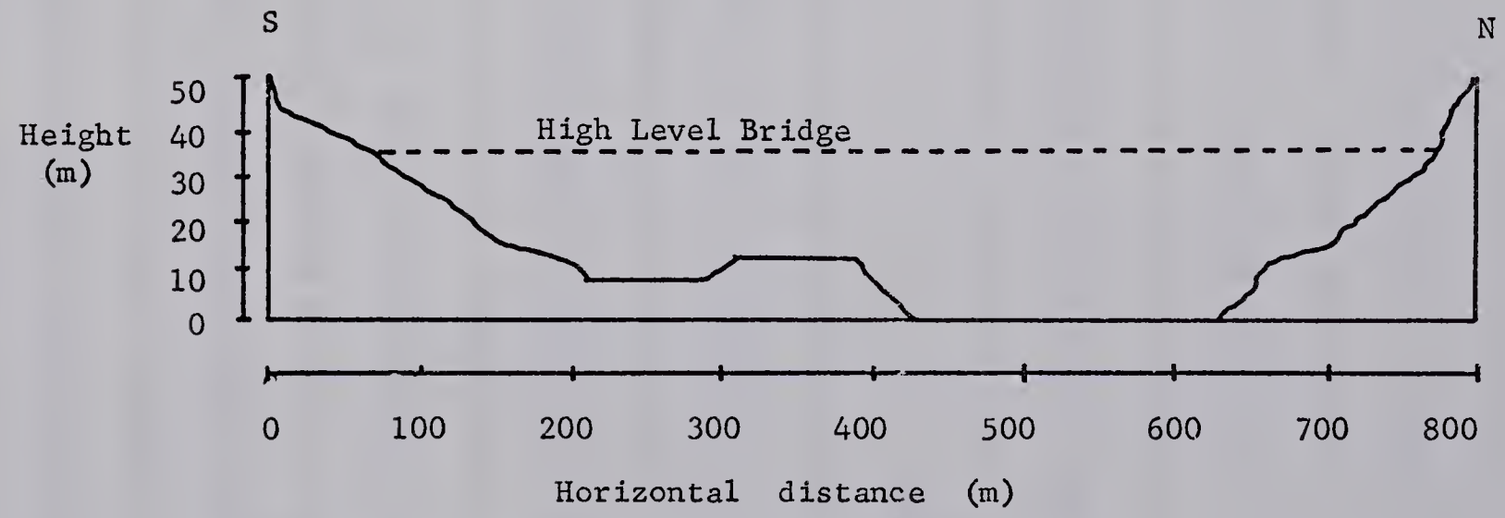

Fig. 3.3 A topographical profile obtained from Fig. 3.2 at the cross-section of North Saskatchewan River Valley along the High Level Bridge.

investigation was performed, gently slopes from WNW down to ESE. A rough indication of the valley floor can be seen in Fig. 3.1 which shows water surface and ice surface profiles along the river. The topographical features of the study area are shown in Fig. 3.2 which is a contour map provided by the City of Edmonton. A profile at the location of the High Level Bridge is shown in Fig. 3.3. However, the elevation of the High Level Bridge above the water surface can not be obtained directly from Fig. 3.3. It is a variable which depends on time and location on the bridge. This is because the bridge is sloped about 0.2 o/o and the water level is changing all the time. For our modelling study, we use the mean elevation for the appropriate season.

3.3 Instrumentation siting

The locations of the instrumentation sites are shown on the contour map in Fig. 3.2. There were six manned meteorological stations and two CO monitor traverse routes established across the North Saskatchewan River Valley, west of the High Level Bridge in Edmonton. Meteorological stations are identified by number in Fig 3.2, and the traverse routes for the air quality monitoring are shown by curve AF for the south bank and curve AD for the north bank of the valley. A description of the general characteristics and equipment for each station follows:

(1) Station 1

This station was situated on the valley rim along the north

bank with no obstructions in the immediate vicinity. It was at an elevation of about 50 m above the water surface of the river. Wind speed, wind direction, and temperature were observed. The meteorological equipment at this station, pictured in Fig. 3.4, were a cup and vane anemometer erected on a tower at 3.7 m and a thermograph placed in a Stevenson screen.

Fig. 3.4 Meteorological equipment located at Station 1 at valley rim of the north bank.

(2) Station 2

Station 2 was located on the valley rim of the south bank, near the Tory Building of the University of Alberta. The meteorological equipment was identical to that of Station 1. It was found that wind data were not useable because of nearby obstructions.

(3) Station 3

Station 3 was located on a gravel bar in the river. The meteorological equipment at this station, pictured in Fig. 3.5, included a three-dimensional propeller anemometer erected at 3.7 m, a thermograph placed in a Stevenson Screen, and a water temperature thermograph. On some occasions CO monitor traverse route AD was extended to Station 3

Fig. 3.5 Meteorological equipment located at Station 3 situated on a gravel bar in the river.

(4) Station 4

Station 4 was located in the middle of the High Level Bridge. The elevation of this station above the water surface of the river was about 42 m. Thermocouples were suspended at four levels at 8 m intervals below the bridge and connected to a multi-channel digital meter as shown in Fig. 3.6. Temperature readings were logged at intervals of 5, 10, or 15 minutes depending on the steadiness of the data.

Fig. 3.6 The equipment for measuring the vertical temperature profile below the High Level Bridge.

(5) Station 5

The location of Station 5 was on the valley slope of the north bank of the valley. The elevation of this station was about 20 m above the water surface of the river. The arrangement of the meteorological

equipment for measurement of slope wind and air temperature is shown in Fig. 3.7

Fig. 3.7 Station 5 located on the north bank slope . A thermograph in a Stevenson screen was located nearby .

(6) Station 6

Station 6 was located in a forest clearing on the slope of the south bank of the river valley. The meteorological equipments was similar to that of Station 5.

3.4 Data collection

3.4.1 Temperature profile

For the modelling computations we need temperature profile data in the valley atmosphere. The use of thermocouples to measure the air temperature is based on the principle that if two or more different metals are joined to form a circuit, there will exist an electromotive force in the circuit if the metals are at different temperatures. Therefore, a current will flow in the circuit and the intensity of the current is proportional to the difference in temperature.

In the investigation, we used thermocouples at different heights below the High Level Bridge in conjunction with a rotary selector switch and a digital thermocouple meter. The precision of the measurement was about 0.05^{o}C. A schematic diagram showing the thermocouple circuit for sequential air temperature measurements is given in Fig. 3.4. The measuring junction was constructed from fine wire (0.005 mm in diameter) in order to minimize radiation error. Chromel-constantan thermocouples were used because of their large sensitivity. The entire circuit was calibrated in the laboratory at several values of temperature within its range. In order to make comparisons of temperature measured by various thermometers, it was necessary to calibrate the thermocouple reading with a reference pychrometer. We have made both laboratory and field experiment calibrations. It was found necessary to add 2.7^{o}C to each thermocouple reading in order to obtain absolute values which represent the true readings in our experiment. After reduction of the raw data, we

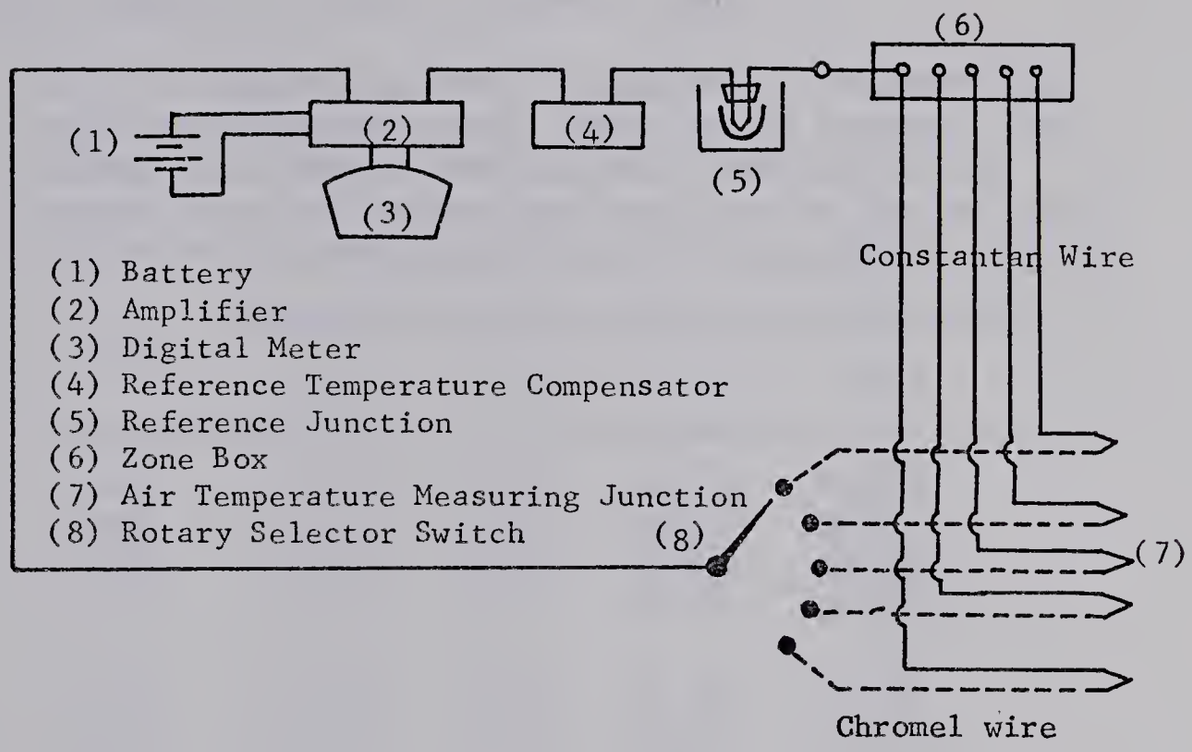

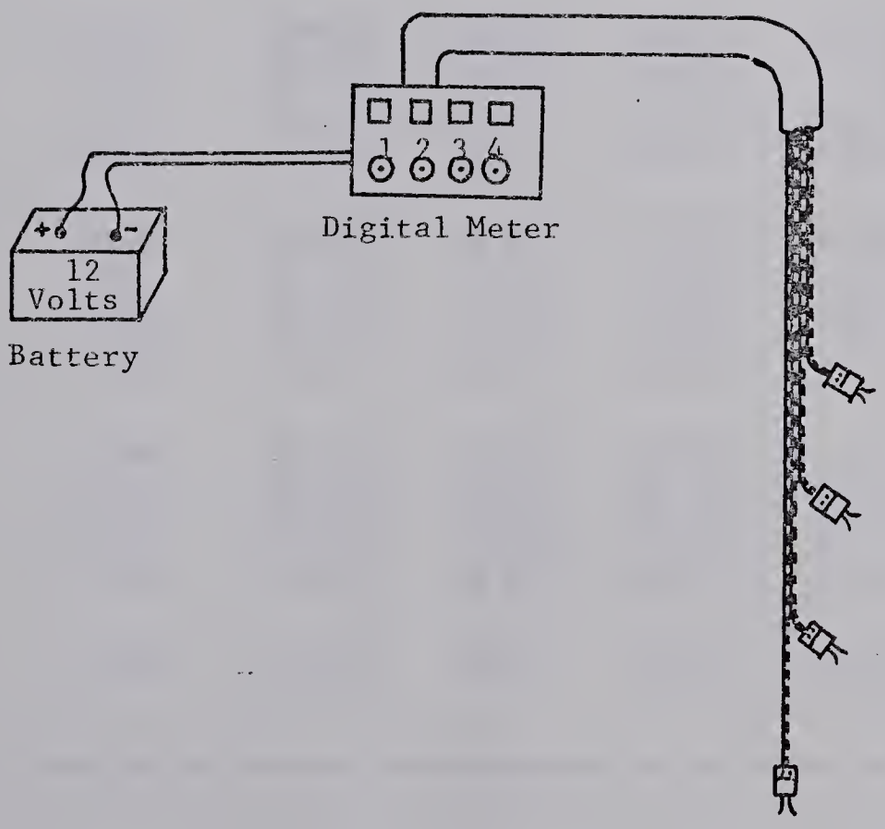

Fig.3.8 Schematic diagram of the thermocouple circuit used for atmospheric temperature profile measurements.

obtain the temperature profile as given in Table 3.1

Table 3.1 Temperature data (^{o}C) measured by thermocouples which were suspended at four levels at 8 m intervals. The readings were derived from 15-mimute averages of the original data. The measurements were made on July 20, 1977.

Time	Elevation above the water surface of river			
	10 m	18 m	26 m	34 m
1900	23.8^{o}C	23.6^{o}C	23.6^{o}C	23.3^{o}C
1915	23.8^{o}C	23.7^{o}C	23.6^{o}C	23.5^{o}C
1930	23.9^{o}C	23.7^{o}C	23.6^{o}C	23.5^{o}C
1945	23.8^{o}C	23.6^{o}C	23.4^{o}C	23.1^{o}C
2000	23.2^{o}C	23.4^{o}C	23.2^{o}C	23.0^{o}C
2015	23.1^{o}C	23.3^{o}C	23.1^{o}C	23.0^{o}C
2030	22.9^{o}C	23.3^{o}C	22.9^{o}C	22.7^{o}C
2045	24.4^{o}C	24.4^{o}C	24.4^{o}C	24.3^{o}C
2100	23.9^{o}C	24.0^{o}C	23.9^{o}C	23.8^{o}C
2115	22.0^{o}C	22.1^{o}C	22.4^{o}C	22.3^{o}C
2130	21.5^{o}C	21.2^{o}C	21.3^{o}C	21.2^{o}C
2145	20.7^{o}C	20.7^{o}C	20.9^{o}C	20.9^{o}C
2200	20.4^{o}C	20.4^{o}C	20.4^{o}C	20.2^{o}C
2215	19.7^{o}C	19.9^{o}C	19.9^{o}C	19.9^{o}C
2230	19.3^{o}C	19.3^{o}C	19.4^{o}C	19.3^{o}C
2245	19.2^{o}C	18.9^{o}C	18.9^{o}C	18.8^{o}C
2300	18.8^{o}C	18.8^{o}C	18.6^{o}C	18.6^{o}C
2315	18.4^{o}C	18.3^{o}C	18.3^{o}C	18.2^{o}C
2330	18.0^{o}C	17.9^{o}C	17.8^{o}C	17.7^{o}C
2345	18.0^{o}C	18.0^{o}C	17.9^{o}C	17.9^{o}C
2400	18.5^{o}C	18.5^{o}C	18.5^{o}C	18.3^{o}C

3.4.2. Wind

Wind data are very important for the modelling computations. Information on wind speeds and directions at the valley top and bottom is needed in order to estimate the wind profile, the diffusion of pollutants from the pollutant sources, the advection of pollutants, etc.. Wind direction was measured by a wind vane (see Fig. 3.4) which utilized a synchro-motor system. The vane was coupled to the shaft of a synchro-transmitter which was connected electrically to the synchro-receiver. The shaft of the synchro-receiver reproduced the rotation of the shaft of the synchro-transmitter and thereby located the vane position. Recording of vane position was accomplished with a potentiometer and a recording voltmeter. The potentiometer contact was coupled to the vane shaft; thus any angular position of the vane corresponds to a particular voltage that can then be applied to a suitably calibrated recording voltmeter. Wind direction measurements are given in Table 3.2 for the Station 1.

Table 3.2 Hourly mean wind directions at Station 1

Variable	Local time 17-18	18-19	19-20	20-21	21-22	22-23	23-24
wind direction	158°	145°	145°	135°	135°	135°	135°

The cup anemometer, pictured in Fig. 3.4, was used to measure the wind speeds at Stations 1, 5, and 6 in our experiment. The number of revolutions in a given time measured by the cup anemometer can be counted

and translated into wind speed by means of calibration data. The anemometer generates electrical impluses which are counted and fed to a frequency measuring circuit that yields a voltage output. The voltage output which is directly proportional to the speed of rotation of the cup wheel, was recorded on a strip-chart recorder.

The Gill propeller anemometers shown in Fig. 3.9 were used to measure three-dimensional wind speeds at Station 3. The cup anemometers and the Gill propeller anemometers were calibrated in the wind tunnel of the Department of Mechanical Engineering, at the University of Alberta, in Edmonton, on July 8, 1977 prior to the experiment. The calibration is shown in Fig 3.9 and Fig 3.10. Calibration data are given in Table 3.3. Calibration curves for each anemometer were fitted by the method of least squares for the range from 1 $m.s^{-1}$ to 10 $m.s^{-1}$. At low speeds nonlinear calibrations were used. The results for the cup anemometers are given in Fig. 3.11. The results for the Gill propeller anomometers at low speeds are shown in Fig. 3.12. Having these calibration charts, we can convert the recorded voltage output into wind speed. We measured the wind speed at valley top and valley bottom in the experiment. After taking hourly averages we obtain the wind data for valley top Station 1 as given in Table 3.4. Similarily, the wind data for Station 3 located at valley bottom are given in Table 3.5.

Table 3.3 Anemometer calibration data from the wind tunnel of the Department of Mechanical Engineering, at the University of Alberta on July 8, 1977.

Run	Speed ($m.s^{-1}$)	Hot film (volts)	Gill (volts)	Station 1 ($m.s^{-1}$)	Station 2 ($m.s^{-1}$)	Station 5 ($m.s^{-1}$)
1	0.0	-[1]	0.00	NT[2]	NT	NT
2	0.29	0.95	0.008	NT	NT	NT
3	0.59	1.95	0.027	NT	NT	NT
4	0.94	3.14	0.046	NT	NT	NT
5	0.97	3.22	0.047	NT	0.85	NT
6	1.12	3.72	0.054	0.98	0.85	NT
7	1.52	5.07	0.074	1.07	0.89	NT
8	1.60	-	0.084	1.34	0.89	NT
9	1.90	-	0.100	1.34	1.34	0.72
10	2.85	-	0.150	3.04	2.01	1.56
11	3.78	-	0.199	4.47	3.35	2.68
12	4.77	-	0.251	5.81	4.69	4.25
13	5.74	-	0.302	7.60	6.26	5.81
14	6.61	-	0.348	9.16	7.82	7.15
15	7.66	-	0.403	11.18	9.39	8.94
16	9.69	-	0.510	14.75	12.74	12.52
17	7.51	-	0.395	10.95	9.16	8.72
18	5.66	-	0.298	7.60	6.04	5.59
19	3.80	-	0.200	4.47	3.35	2.68
20	2.83	-	0.149	3.13	2.01	1.34
21	1.82	-	0.096	1.70	0.85	0.45
22	1.53	5.09	0.074	1.34	0.67	0.22
23	1.23	4.09	0.059	1.12	0.54	NT
24	0.91	3.04	0.044	1.12	0.45	NT
25	0.62	2.07	0.029	NT	NT	NT
26	0.32	1.05	0.011	NT	NT	NT
27	0.15	0.50	NT	NT	NT	NT

Notes: 1. - represents hot film is off.

2. NT represents anemometer is not turning.

3. Factory calibration were used for the Gill propeller anemometer at speeds above 1.5 $m.s^{-1}$.

Fig. 3.9 The calibration of cup and Gill propeller anemometers in the wind tunnel of the Department of Mechanical Engineering, the University of Alberta on July 8, 1977.

Fig. 3.10 Wind speed data recorders for anemometer shown in Fig. 3.9.

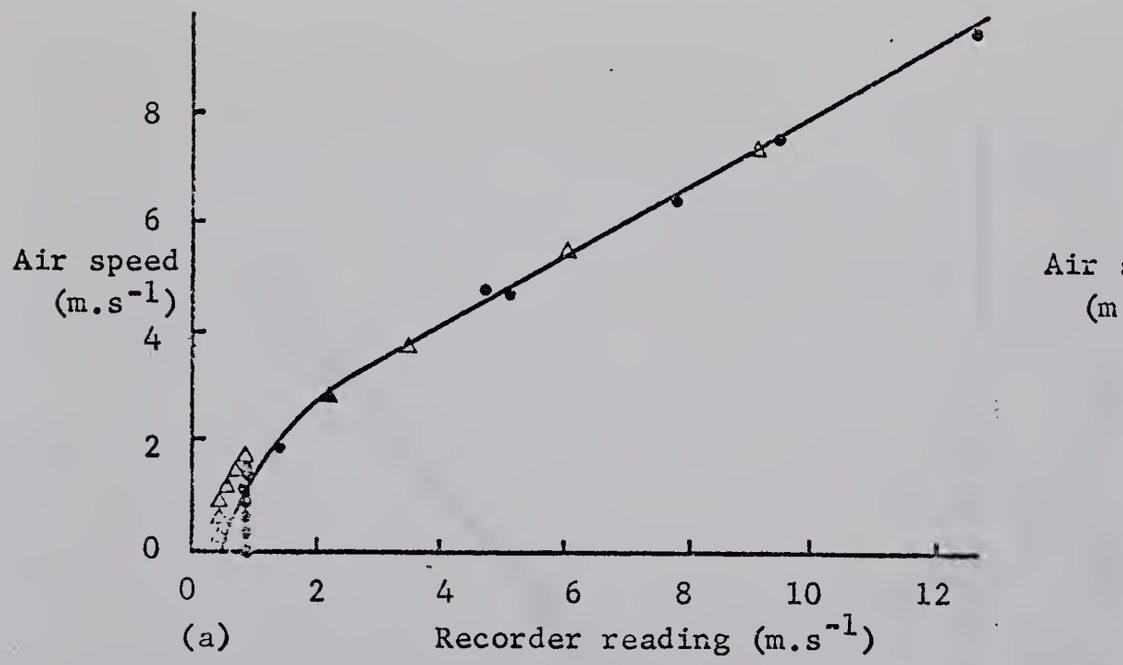

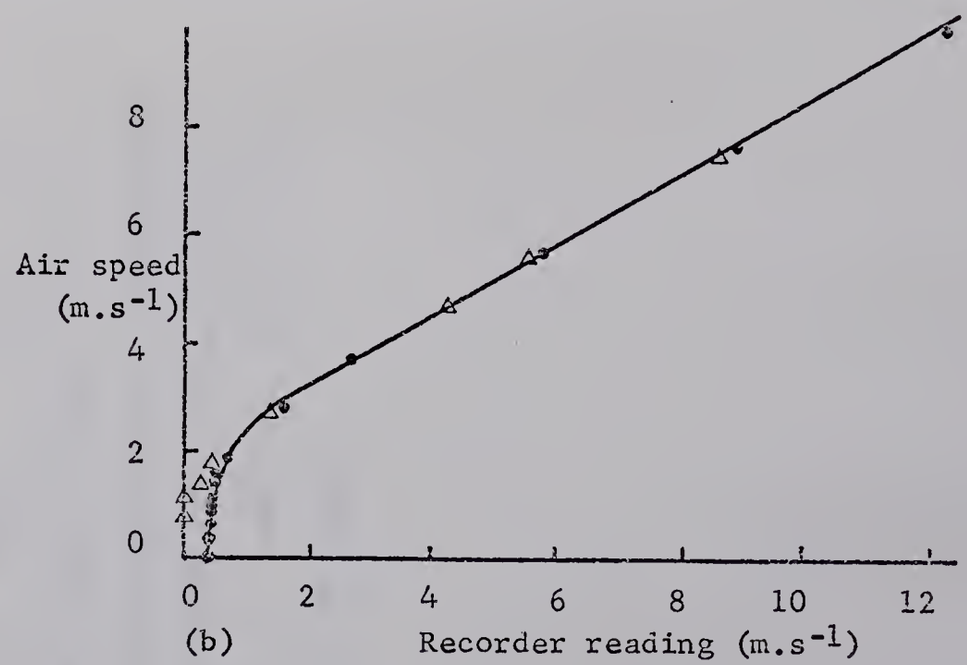

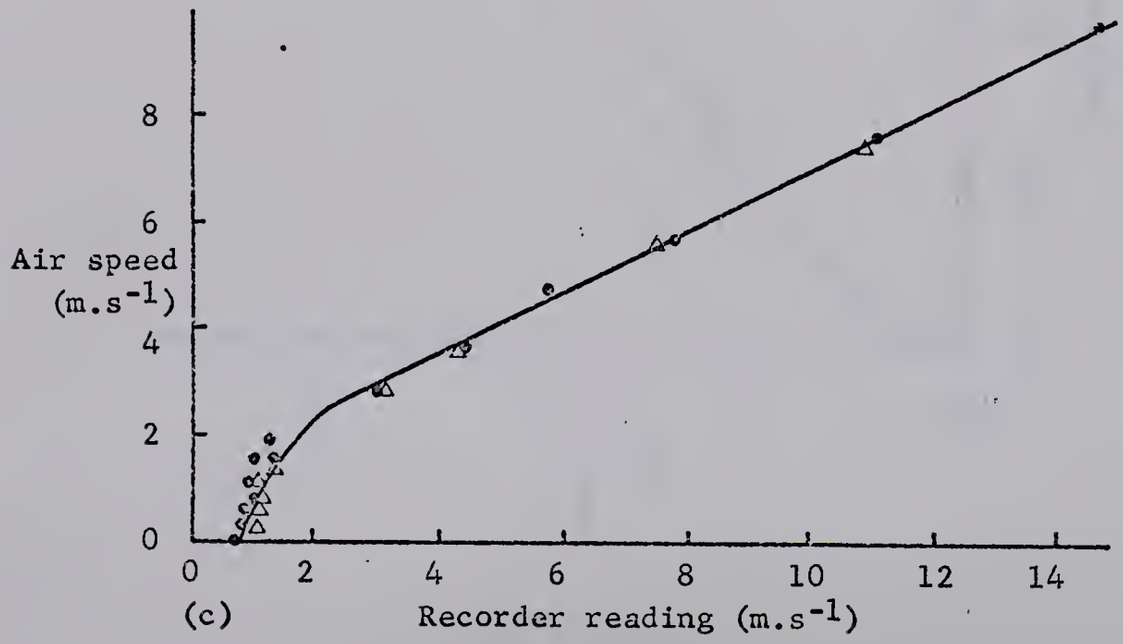

Fig. 3.11 Calibration charts for cup anemometers at Stations 1, 2, and 5 which are shown in (a), (b), and (c) respectively where . means data obtained from increasing wind tunnel air speed and △ means data obtained from decreasing wind tunnel air speed.

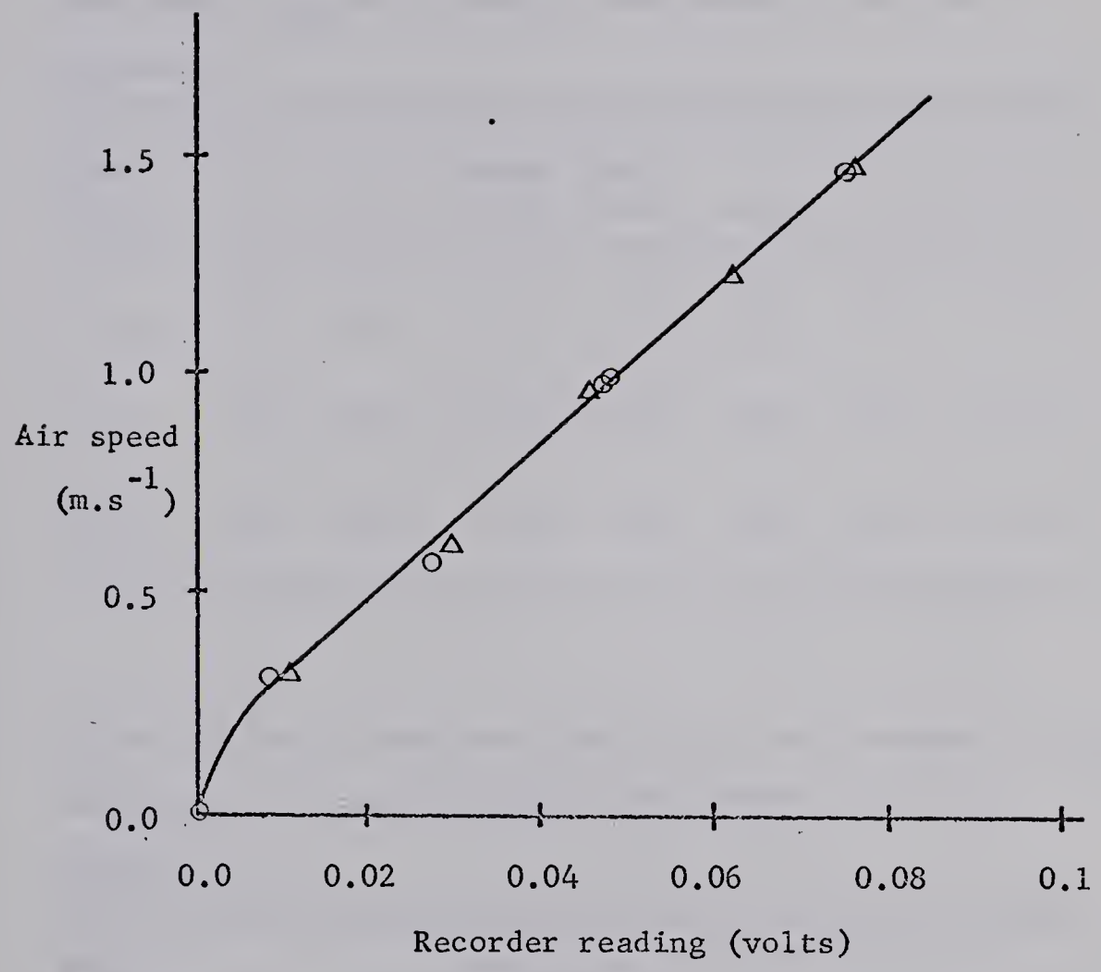

Fig. 3.12 A calibration chart for Gill anemometer, where o means data obtained from increasing wind tunnel air speed and Δ means data obtained from decreasing wind tunnel air speed.

Table 3.4 Hourly mean result (V_{50}) and component (u_{50}, east-west; v_{50}, north-south) wind speeds ($m.s^{-1}$) at Station 1.

Wind speed	Local time 17-18	18-19	19-20	20-21	21-22	22-23	23-24
V_{50}	4.7	5.4	6.1	5.1	3.9	3.3	3.9
u_{50}	-1.9	-3.1	-3.5	-3.6	-2.8	-2.4	-2.8
v_{50}	4.5	4.4	5.0	3.6	2.8	2.4	2.8

Table 3.5 Hourly mean resultant ($V_{3.7}$) and component ($u_{3.7}$, east-west; $v_{3.7}$, north-south) wind speeds ($m.s^{-1}$) at Station 3.

Wind speed	Local time 17-18	18-19	19-20	20-21	21-22	22-23	23-24
$V_{3.7}$		3.4	3.2	1.9	1.2	1.4	1.6
$u_{3.7}$		-3.1	3.0	-1.7	-0.7	-1.0	-1.3
$v_{3.7}$		1.4	1.3	0.7	0.9	0.9	1.0

3.4.3 Temperature

Temperatures were measured at Station 1, 3, 5, and 6 by thermographs in Stevenson Screens as pictured in Fig. 3.4. Thermographs are based on the principle that two metallic strips of materials having different thermal-expansion coefficients when welded together will form a unit which will bend with a change in temperature. If one end of the unit is fixed in position, the other end can be used for recording the ambient temperature. In order to make the comparisons of the temperature data taken from various thermographs, we have made numerous calibrations of all thermographs at various temperatures with the following results

Table 3.6 Results of calibrations of all thermographs used in the experiment work.

Station	Error (To be added to chart reading)
1	$-0.019^{o}C\ \bar{T} - 0.094^{o}C \pm 0.1^{o}C$
3	$0.2^{o}C \pm 0.1^{o}C$
5	$-6.7^{o}C \pm 0.2^{o}C$
6	$-5.3^{o}C \pm 0.3^{o}C$
River water	$8.7^{o}C \pm 0.2^{o}C$

where $\bar{T}$ is the ambient temperature at Station 1. Calibrated temperatures for the four stations at 15 min. intervals are listed in Table 3.7. Table 3.7 seems to show a strong inversion over Station 6 but no inversion on the north side of the river except between Station 1 and 5 from 2100 to 2145 and between Station 3 and 5 from 1700 to 1715.

Table 3.7 Calibrated thermograph data for Experiment 2

Time (MDT)	Station temperature (°C)			
	1	3	5	6
1700	23.2	23.0	23.2	23.5
15	22.9	23.4	23.5	22.5
30	23.2	23.5	22.6	22.6
45	22.3	23.2	22.7	21.9
1800	22.5	23.6	23.6	21.9
15	23.2	23.9	23.5	21.9
30	23.1	24.2	23.5	22.0
45	23.3	24.1	23.4	21.6
1900	23.3	24.0	23.5	21.0
15	23.1	24.0	23.3	20.9
30	23.1	24.2	23.2	20.5
45	22.9	23.9	23.0	20.4
2000	22.8	23.7	22.6	19.8
15	22.4	23.5	22.2	18.9
30	22.2	23.1	21.9	18.4
45	21.8	22.8	21.5	17.8
2100	21.3	22.2	21.1	17.4
15	21.0	21.6	20.7	16.9
30	20.3	20.9	20.2	16.3
45	19.8	20.2	19.7	15.7
2200	19.4	19.6	19.6	15.3
15	19.1	19.2	19.2	14.9
30	18.7	19.0	18.9	14.6
45	18.4	18.8	18.5	14.2
2300	18.1	18.5	18.2	14.0
15	17.5	18.1	17.7	13.7
30	17.3	17.6	17.5	13.5
45	17.3	17.5	17.5	13.3
2400	17.6	17.7	17.5	13.0

3.4.4 CO-concentration

The CO-concentration measurements were taken by two people carrying the CO-analyzers and walking up and down the valley bank along the traverse route shown in Fig. 3.2 . The portable CO-analyzers were subject to major zero drift. Laboratory measurements using N_2 gas free of CO showed that the zero drift was a smooth curve with a time constant of the order of several hours. In experiments 1 and 2 attempts were made to zero the CO-analyzers in the field using portable cylinders of N_2 gas. However, these attempts failed because the N_2 gas contained an unacceptable residual of a few tenths of one ppm of CO.

Experience in the field showed that CO values were highly variable with time constants of minutes to tens of minutes in contrast to the behaviour of zero drift. Furthermore, during traverses several apparent zero readings characterized by low-amplitude noise only were found. These minima were used to construct zero curves as shown in Figs. 3.13 and 3.14. The departures of the actual recorder trace from the assumed zero curves were accepted as true CO concentration. It is possible that the CO concentrations determined in this way are systematically too low but the relative values from station to station and from time to time should be reliable.

The CO-analyzers were calibrated in the laboratories of the Air Pollution Division of Alberta Environment immediately prior to each field experiment. At this time the instrument was adjusted if necessary

to yield the correct CO concentration on the strip-chart recorders that were used in the field. Check calibrations were carried out immediately after the field experiments. No significant span drift was noted over periods of several weeks. Occasional short gaps in data occurred because connectors were loosened during traverses. In addition, it was necessary to change to external batteries for the recorders during the course of each experiment. From five or six readings at each point along the traverses as indicated in Fig. 3.2 , we can construct a diagram showing the variation of CO-concentration with time by extrapolating values between consecutive readings. The results are given in Fig. 3.15 to Fig. 3.23. From these diagrams we can estimate the hourly mean CO-concentration for each site for our numerical computations. These mean values are given in Table 3.8 for the time period 2000 to 2400 when the surface-based inversion was present and the conditions satisfied the requirements of our box model as discussed in Chapter IV.

Table 3.8 Hourly mean CO-concentrations (ppm) derived from data in Fig. 3.15 to Fig. 3.23

Time	North slope					South slope			
(MDT)	A	B	C	D	E	A	B	C	D
20-21	0.29	0.20	0.24	0.24	0.86	0.13	0.07	0.18	0.12
21-22	0.21	0.18	0.15	0.40	0.79	0.30	0.06	0.18	0.10
22-23	0.15	0.13	0.06	0.37	0.82	0.34	0.07	0.20	0.07
23-24	0.19	0.06	0.08	0.18	0.60	0.29	0.07	0.13	-

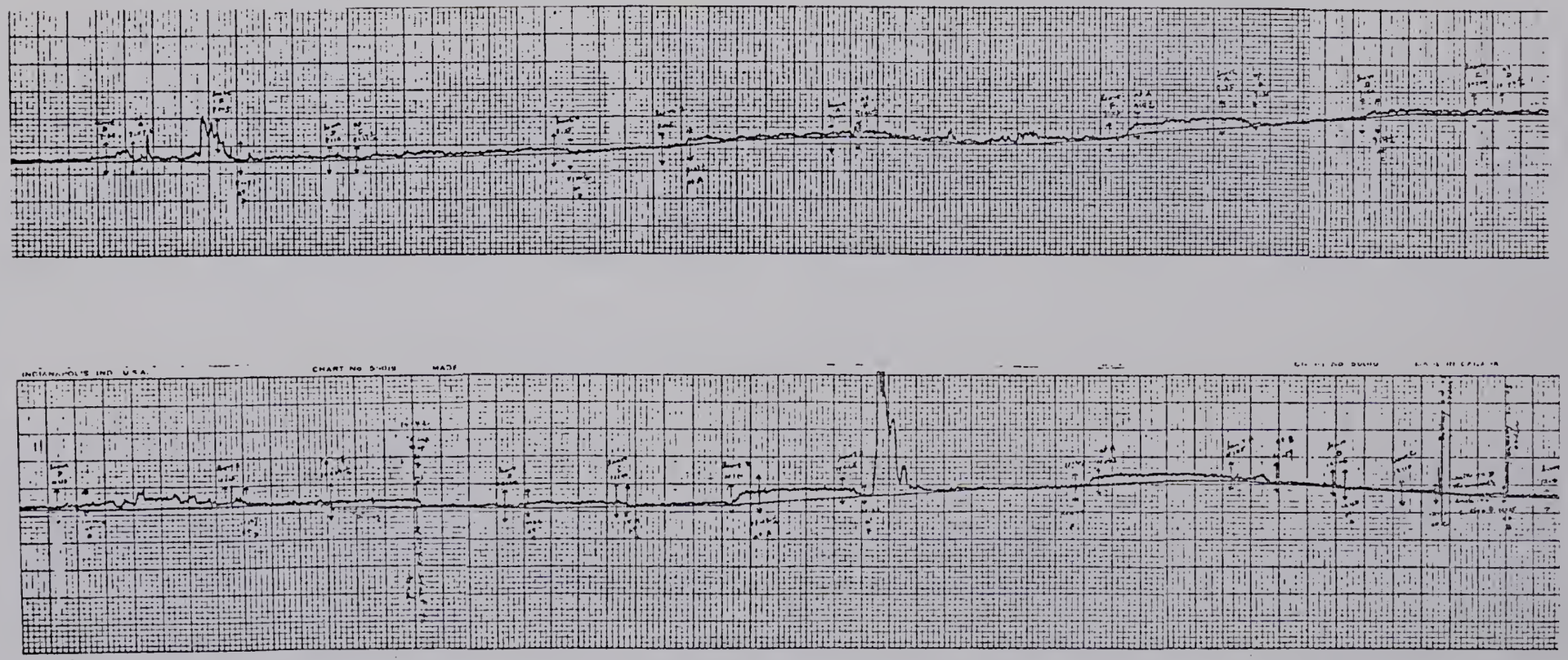

Fig. 3.13 CO-concentration data obtained from the portable CO-analyzer over the south slope of North Saskatchewan River Valley during time period 2000-2400, on July 20, 1977. Time scale 0.5 min./div. and CO-concentration scale 0.02 ppm/div..

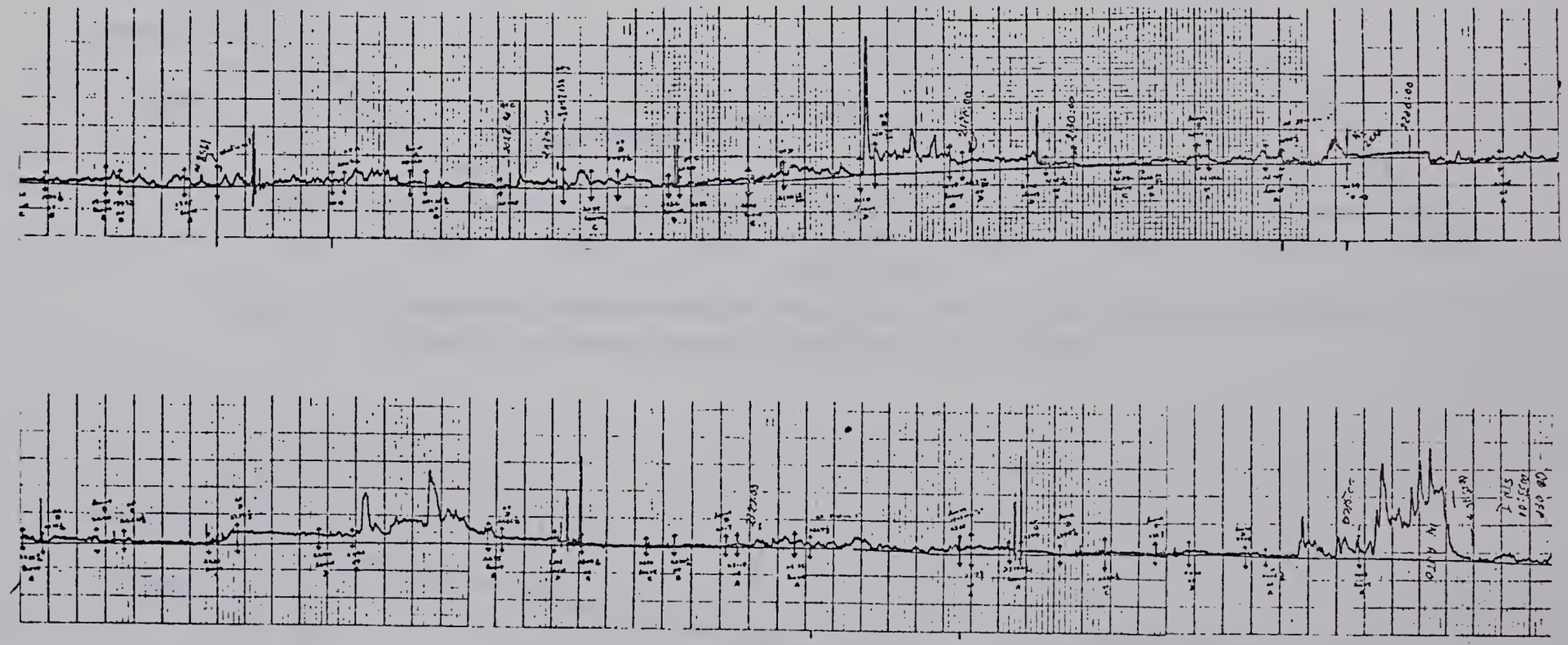

Fig. 3.14 CO-concentration data obtained from the portable CO-analyzer over the north slope of North Saskatchewan River Valley during time period 2000-2400, on July 20, 1977. Time scale 0.5 min./div. and CO-concentration scale 0.02 ppm/div..

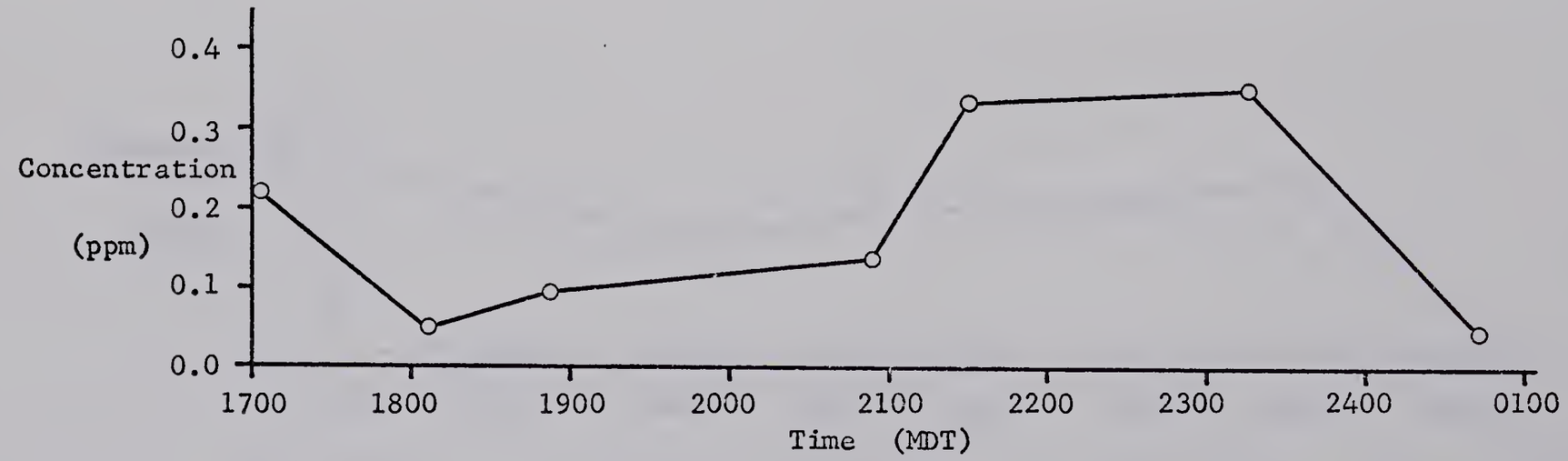

Fig. 3.15 CO-concentration measured at point A of south slope at elevation of about 11 m above the water surface of the river.

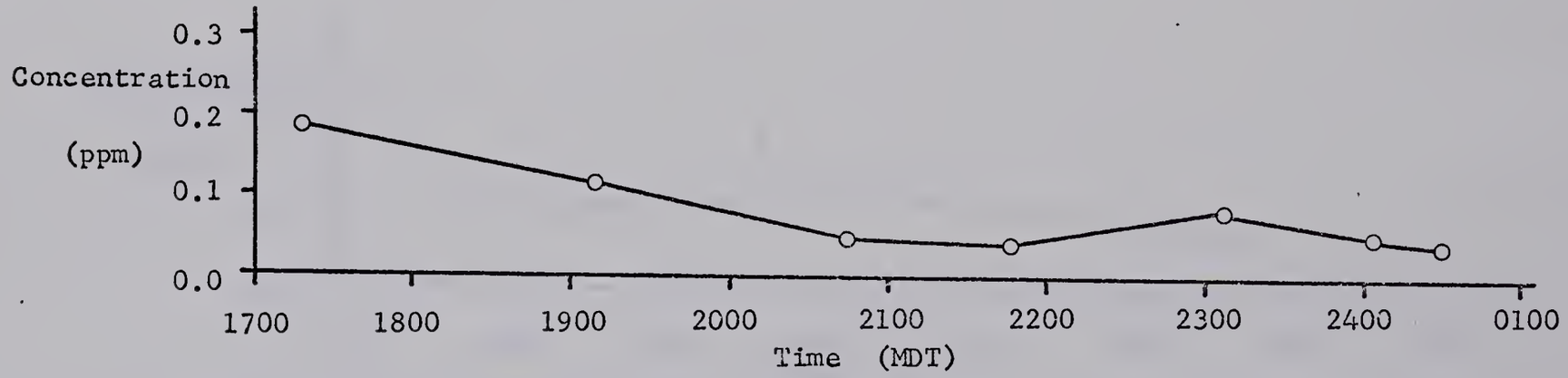

Fig. 3.16 CO-concentration measured at point B of south slope at elevation of about 20 m above the water surface of the river.

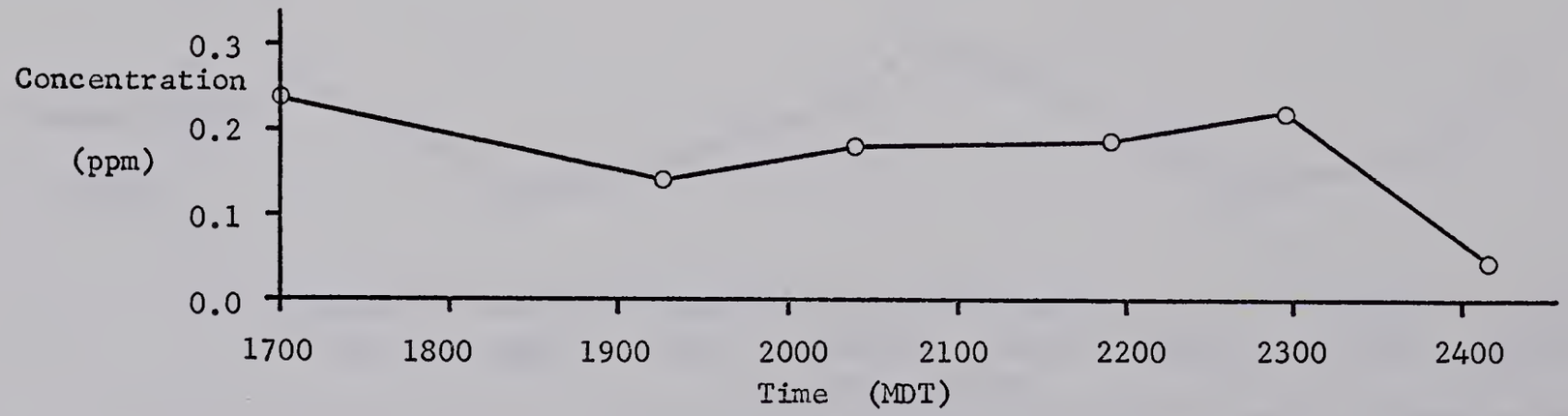

Fig. 3.17 CO-concentration measured at point C of south slope at elevation of about 34 m above the water surface of the river.

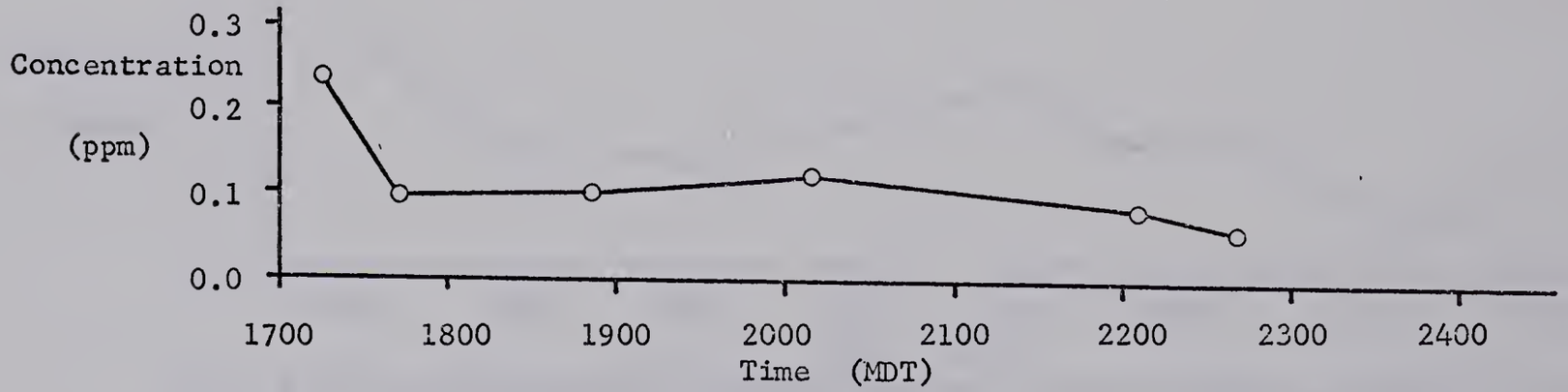

Fig. 3.18 CO-concentration measured at point D of south slope at elevation of about 40 m above the water surface of the river

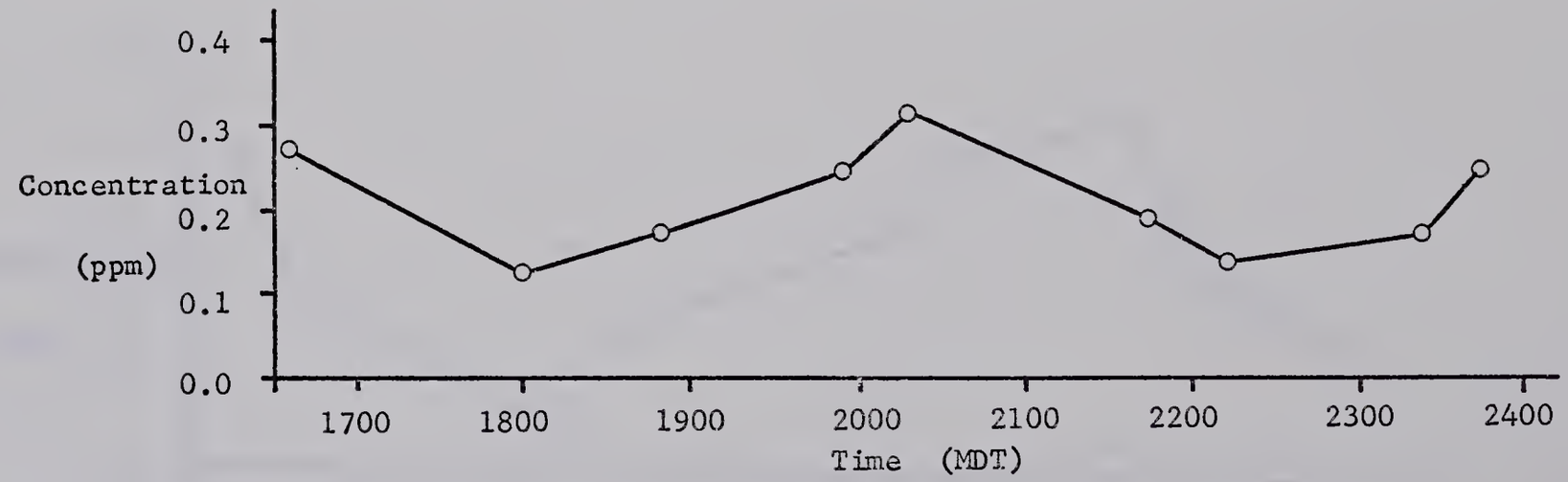

Fig. 3.19 CO-concentration measured at point A of north slope at elevation of about 44 m above the water surface of the river.

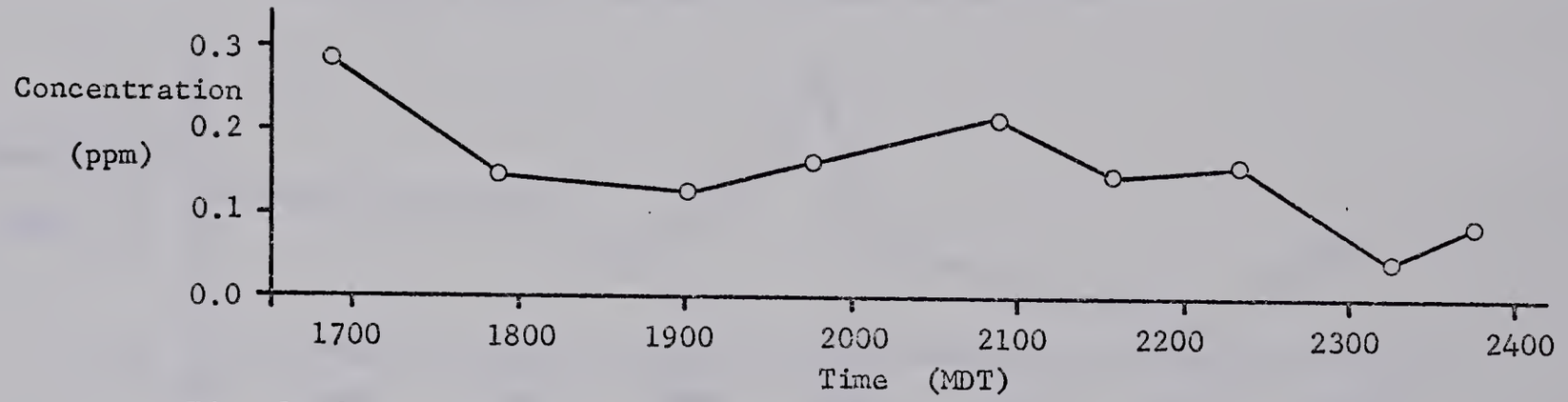

Fig. 3.20 CO-concentration measured at point B of north slope at elevation of about 38 m above the water surface of the river.

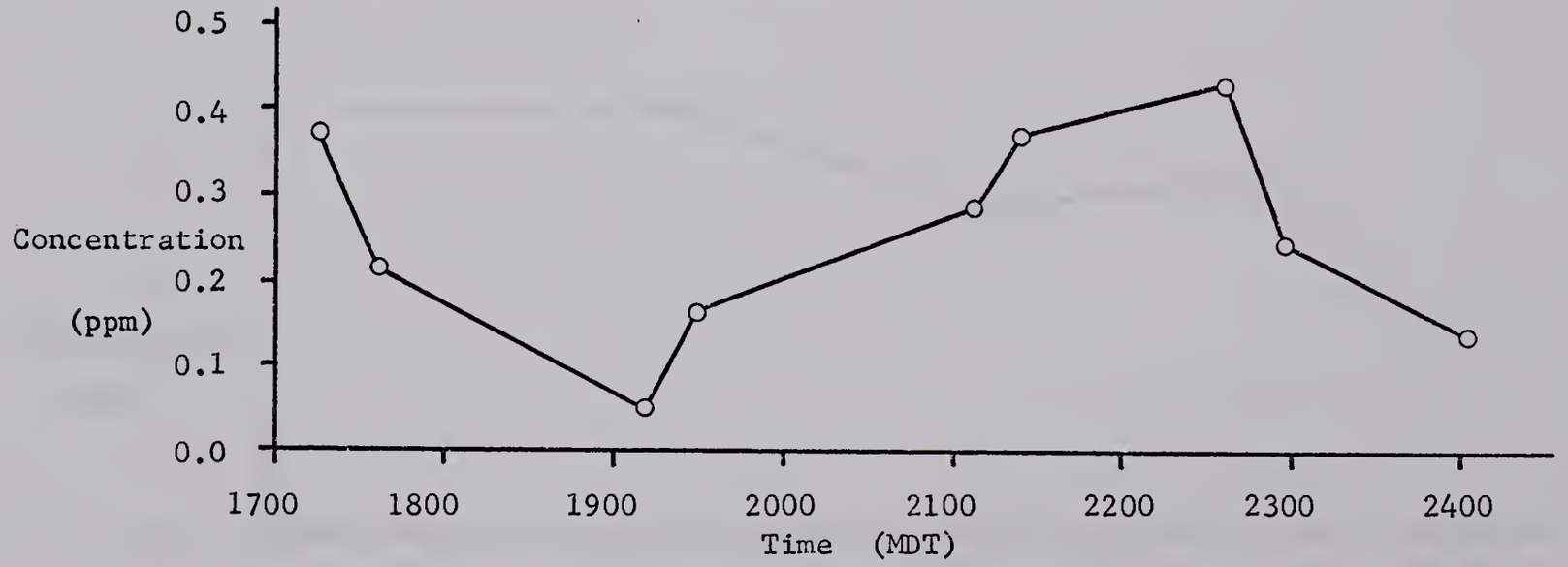

Fig. 3.21 CO-concentration measured at point D of north slope at elevation of about 10 m above the water surface of the river.

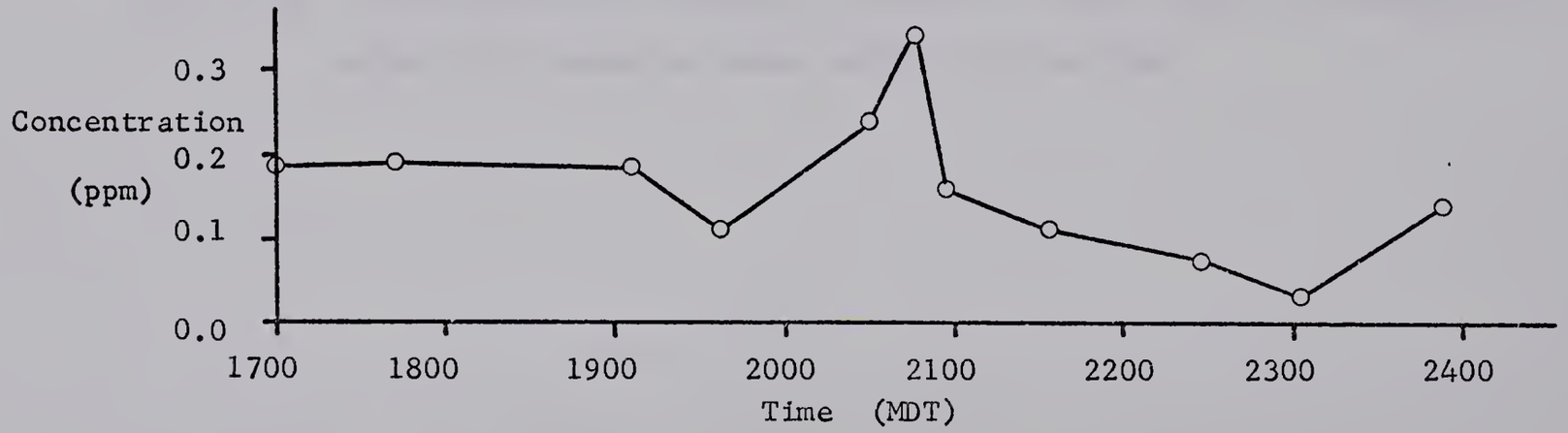

Fig. 3.22 CO-concentration measured at point C of north slope at elevation of about 12 m above the water surface of the river.

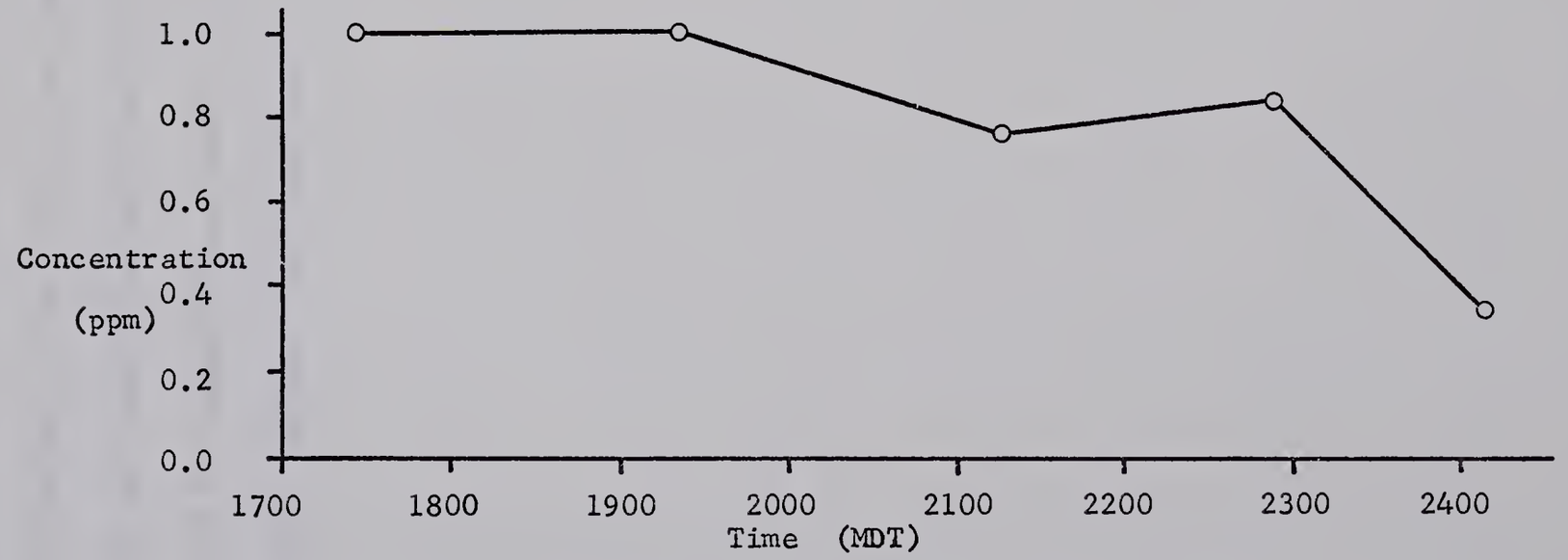

Fig. 3.23 CO-concentration measured at point E of north slope at elevation of about 10 m above the water surface of the river.

It is stressed here that we are mostly concerned with the trend rather than absolute values of CO-concentrations in Box 1 for comparison of our modelling computations with the results derived from field measurements. In Chapter IV we find the computational results are in reasonable agreement with the results derived from field data.

3.4.5 Source strength

In our study the pollutant sources within Box 1 were the 105th Street Bridge and River Valley Road. It is very difficult to get a very good estimate of source strength, because it depends on some poorly defined factors such as the localized mean emission factor for a particular year and the traffic flow for the day when the experiment was carried out. In order to simulate the traffic flow data for our purposes it is necessary to use traffic flow counts that were made at these locations on weekdays prior to the experiment. Short-period traffic counts on River Valley Road during several field experiments were within 10 percent of the official counts. In order to calculate a motor vehicle emission factor we need information on vehicle age distribution, climate conditions of the region, average vehicle maintenance , driving habits in the region, etc.. There are many techniques for calculation of the local mean emission factor for different regions and different years. We will follow the method suggested by Taylor (1973). His method is designed for calculating the emission factor for Canada. The required information and formula for the calculation are attached to this text in Appendix A. This method was used to obtain the emission factor for Edmonton for 1977. Having the emission factor, we can calculate the source strength by the following equation:

$$Q_1 = 1.726 \times 10^{-7}.(E.F.).(T.V.) \qquad (3.10)$$

where Q_l is the line source strength, E.F. is the emission factor, and T.V. is the traffic volume. This equation was suggested by Zimmerman (1974). The emission factor was 79.11 gm.mile^{-1}.s^{-1} (49.4 gm.km^{-1}.s^{-1}) using a nationwide average for Canada during 1977.

The traffic flow data required for our calculation were obtained from the Engineering Department, City of Edmonton. Hourly averages are given in Table 3.9 for the line sources within Box 1.

Using the data given in Table 3.9 we can construct traffic flow patterns as shown in Fig. 3.24 and Fig. 3.25 for the 105th Street Bridge and for River Valley Road, respectively. The flow patterns given in these diagrams are for weekdays. It is assumed that they are valid for any weekday in 1977. Therefore, the emission factor and the data in Table 3.9 can be combined to estimate source strengths for the two roadways for the hours of interest in Experiment 2. Hourly mean source strengths for the late evening when inversion condition were observed are listed in Table 3.10.

Table 3.9 Traffic flow data for 105th Street Bridge and River Valley Road which are considered as line sources within our Box 1. (Source: Engineering Department, City of Edmonton, Alberta, Canada)

Time	105th Street Bridge		River Valley Road	
	Number of cars	P(o/o)	Number of cars	P(o/o)
0100	469	0.013	194	0.011
0200	204	0.006	88	0.006
0300	125	0.004	50	0.003
0400	56	0.002	42	0.002
0500	64	0.002	54	0.004
0600	117	0.003	118	0.008
0700	780	0.022	413	0.027
0800	2400	0.066	1302	0.084
0900	2441	0.067	1111	0.072
1000	1921	0.053	748	0.048
1100	1798	0.050	754	0.049
1200	2066	0.057	841	0.054
1300	2268	0.063	853	0.055
1400	2343	0.065	950	0.061
1500	2297	0.063	948	0.061
1600	2551	0.070	1084	0.070
1700	2813	0.078	1414	0.091
1800	2514	0.069	1141	0.074
1900	2215	0.061	843	0.054
2000	1921	0.053	676	0.044
2100	1302	0.036	505	0.033
2200	1429	0.039	492	0.032
2300	1311	0.036	464	0.030
2400	813	0.022	414	0.027

Table 3.10 Source strengths of the 105th Street Bridge and River Valley Road for selected hours.

Time step	Source strength ($gm.s^{-1}.m^{-1}$)	
	105th Street Bridge	River Valley Road
20-21	0.018	0.0069
21-22	0.020	0.0067
22-23	0.018	0.0063
23-24	0.011	0.0057

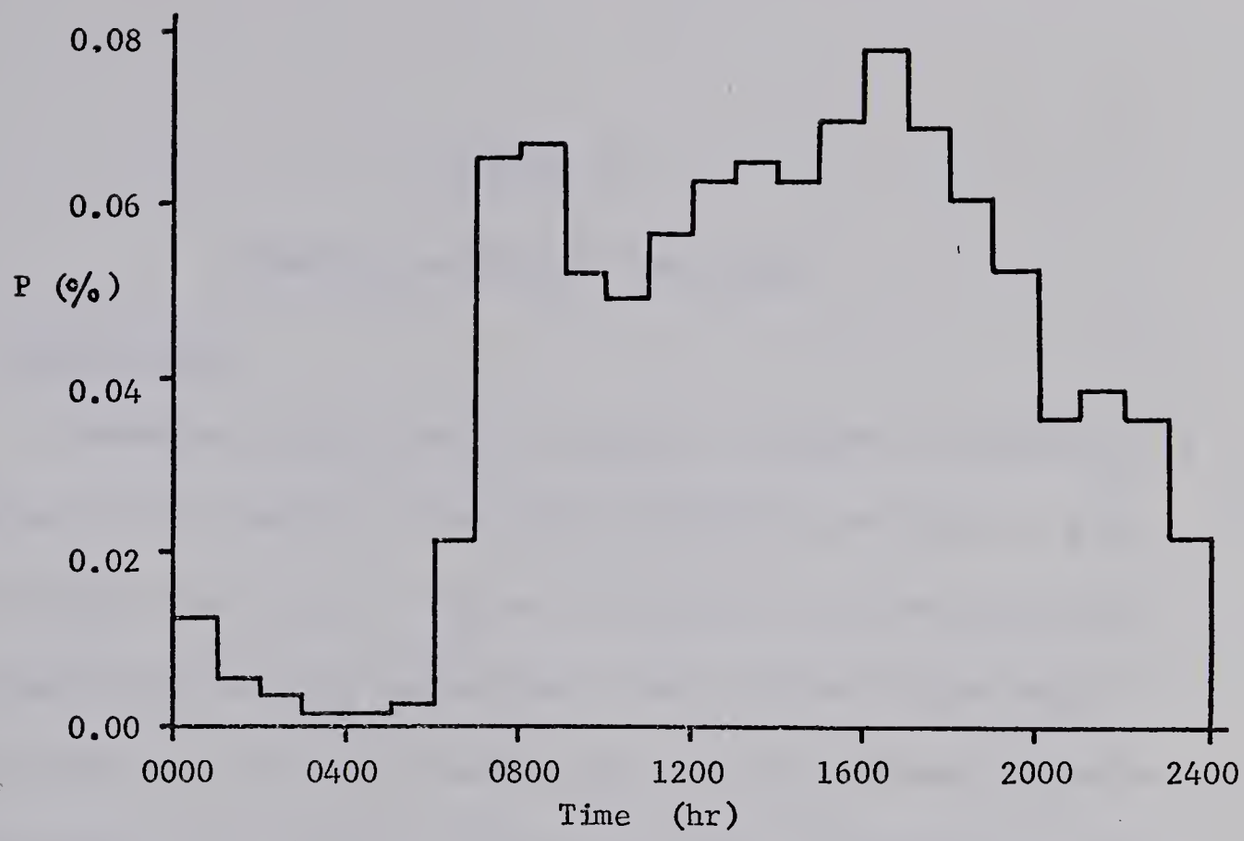

Fig. 3.24 Traffic flow pattern for the line source along 105 th Street Bridge, showing the percentage of daily traffic (P) experienced during a given weekday.

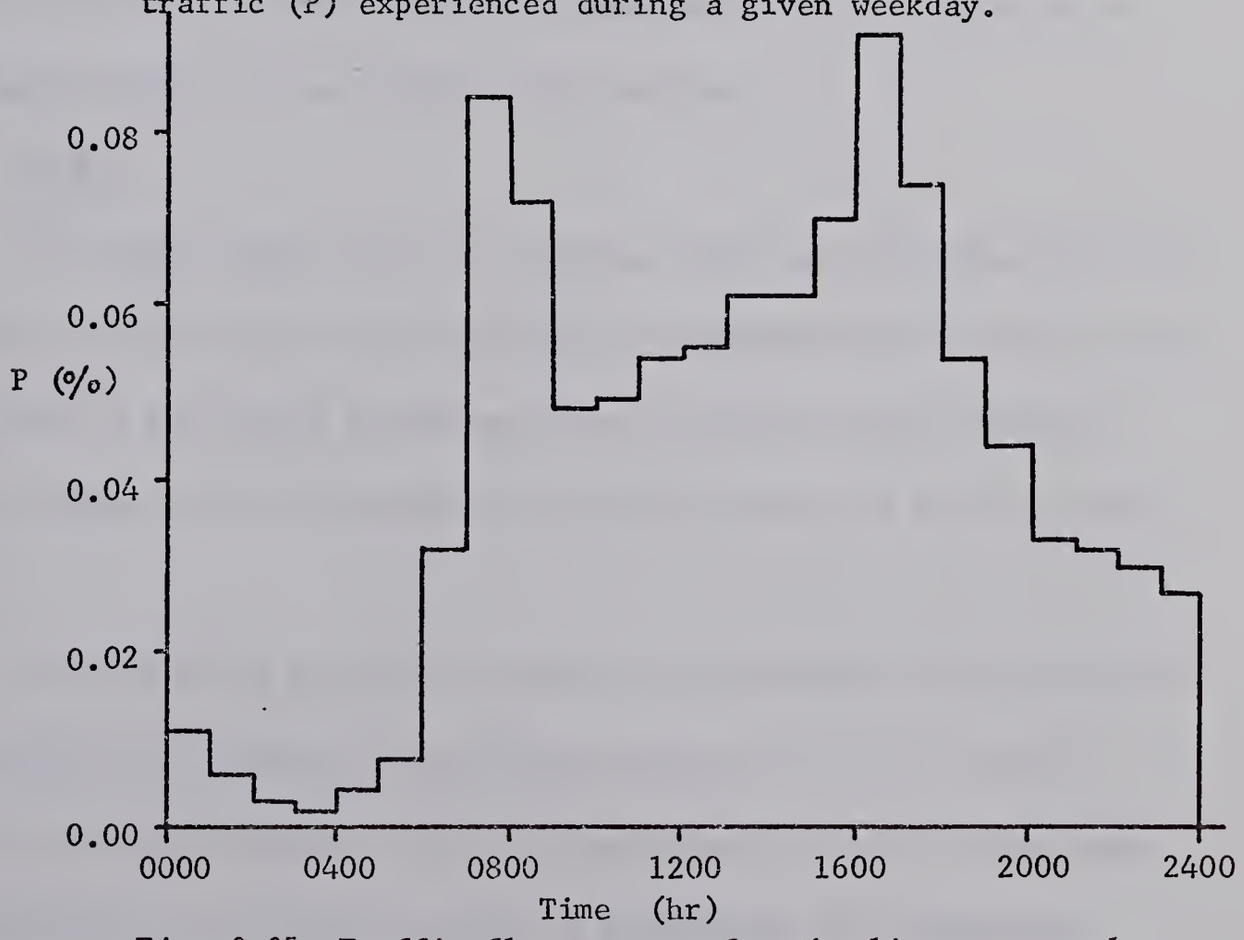

Fig. 3.25 Traffic flow pattern for the line source along River Valley Road, showing the percentage of daily traffic (P) experienced during a given weekday.

CHAPTER IV

NUMERICAL MODELLING COMPUTATION

4.1 Introduction

A numerical application of the model developed in Chapter II is presented in this Chapter. All of the calculations are based on a box model in which the height of the box is the top of the surface-based inversion rather than the conventional identification of box height with the depth of the surface mixing layer. A surface-based inversion commonly exists in the valley region during the nighttime hours. The calculations are consistent with the observations of accumulation of pollutants within the box during these periods.

4.2 The box

The boxes chosen for our modelling study are such that Box 1 is located over the valley bottom during the nighttime hours when cold air sinks down to the valley bottom and forms a surface-based inversion which is taken to be the height of our Box 1, and Box 2 is just above Box 1.

For modelling purposes, we need the dimensions of Box 1 such as its height h, the measure of its ends crossing the valley, and the length of its top boundary. Box 1 has an irregular shape so that some simplifications are needed in order to approximate its dimensions. These simplifications are :

(1) A representative value of the measure A of the cross-section area is estimated and assumed to be constant for that part of the cross-valley section containing the High Level Bridge. This assumption may not be far from the actual situation because in our study region cross-sectional areas are nearly invariant, i.e., the contour lines are more or less parallel, as can be judged from Fig. 4.1.

(2) A representative value of the measure A_h of the top boundary plane of our Box 1 is assumed to be $A_h = L \times w_t$ where L is the length of Box 1 and w_t is the width of the top boundary of A.

(3) A representative value of the measure of the volume of Box 1 can be obtained from the equation $V = A_h \times L$.

Numerical values of the characteristic dimensions of Box 1 can be obtained from the contour line map as shown in Fig. 4.1 and from the temperature-profile measurements for the valley atmosphere at Station 4. A detailed cross-section of the area A can be extracted from Fig. 4.1. This is shown in Fig. 4.2. A plan view of Box 1 and its coordinates chosen for the study, as well as the line sources within it are given in Fig. 4.3. A summary of the data required for the modelling computation is given in Table 4.1. Note that all of these data are hourly-mean values.

Other general features of Box 1 which are very important for the simplification of our modelling equation to a practical form for our study area are:

Fig. 4.1 A contour line map of the region between High Level Bridge and 105th Street Bridge, from which we can extract some geometrical characteristics of Box 1. (Source: Engineering Department, City of Edmonton, Alberta, Canada)

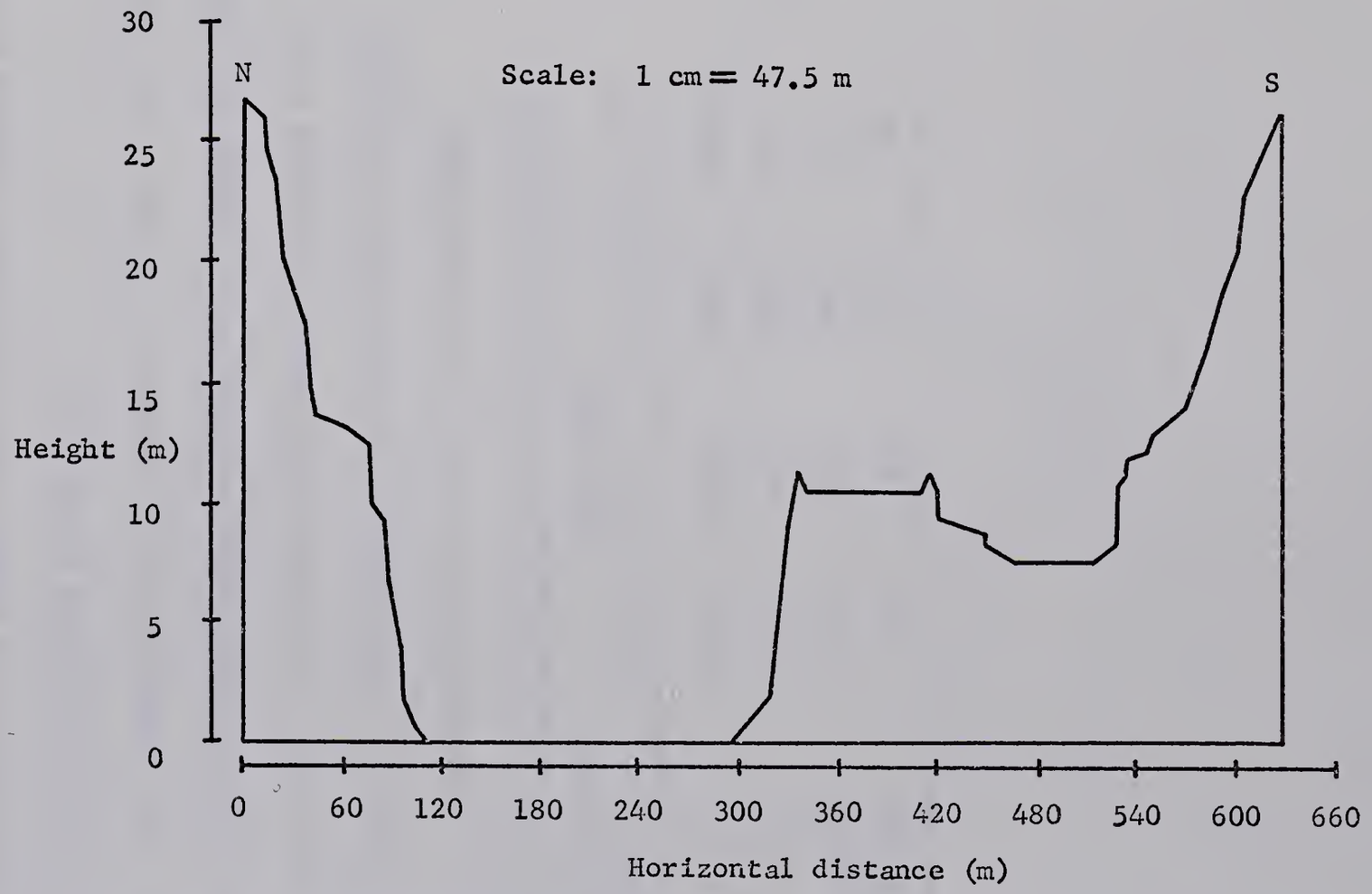

Fig. 4.2 Detailed cross-section characteristics of the area A of Box 1, which is extracted from Fig. 4.1 for the section coincident with the High Level Bridge. Vertical exaggeration 14.6 x.

(1) Box 1 is located just to the west of a right-angle bend in the valley. Because the wind direction was nearly parallel to the valley in Experiment 2, we assume that no pollutants entered Box 1 from the east end AB as shown in Fig. 4.3.

(2) Box 1 has an open section which is labeled AC in Fig. 4.3 so that we may take the pollutants coming out from Box 1 through this open boundary into account. Pollutants will come out from this open boundary, if there is wind component in cross-valley direction.

Table 4.1 Characteristics of Box 1 for the modelling computation.

Characteristics of Box 1	Time (MDT) 20 - 21	21 - 22	22 - 23	23 - 24
A (m^2)	7741.1	9505.6	9505.6	4953.9
L (m)	650	650	650	650
w_t (m)	577	596	596	539
h (m)	20	23	23	15

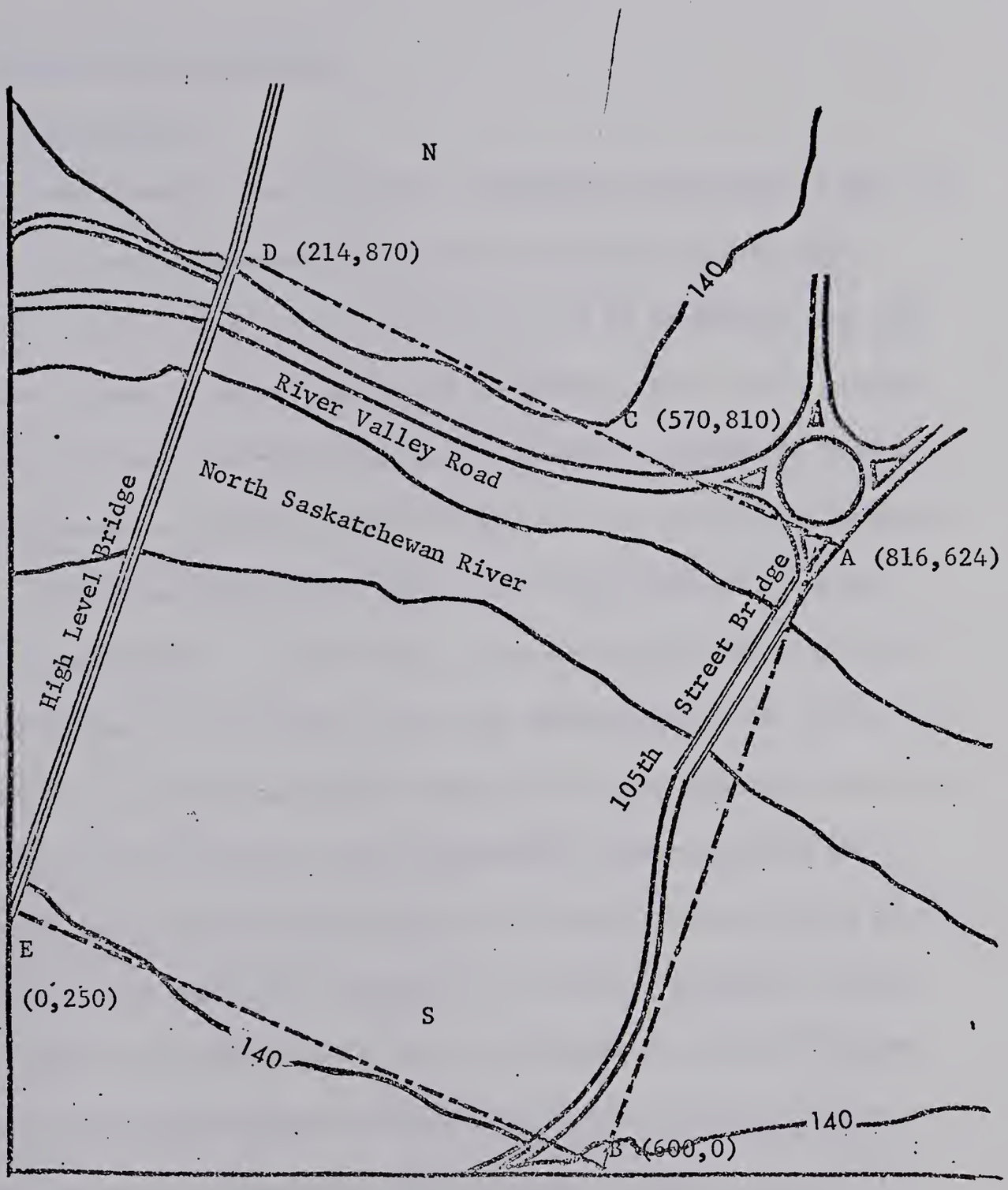

Fig. 4.3 A plan view of Box 1 and the coordinates chosen for this study.

4.3 Computational procedure

4.3.1 The problem

Traditionally, the box model is applied to a box which takes the base of an elevated atmospheric temperature inversion as its upper boundary, the so-called "lid" of the box, and it is assumed that the pollutant concentration within the box is uniform, i.e., it is assumed that the pollutants within the box are well mixed. A schematic view of the traditional box model is shown in Fig. 4.4. If the surface inversion layer is under the upper mixing layer, it is not clear that the box model is appropriate. In our study, a line pollutant source is located near the bottom of the valley so that the situation depicted in Fig. 4.5 may happen. This would be expected especially during the nighttime hours when cold air drains down to the valley bottom. After carrying out a series of calculations using the modelling equations developed in previous chapters of this thesis for this kind of situation, we obtain results which show us that the box model is still effective in this situation. However, the detailed spatial distribution of the pollutant can not be obtained by using the box model. The box model is useful only for the study of time variation in the pollutant concentration. It is not necessary for this purpose to know the detailed spatial distribution of pollutants within the box.

4.3.2 Modelling equation for our study area

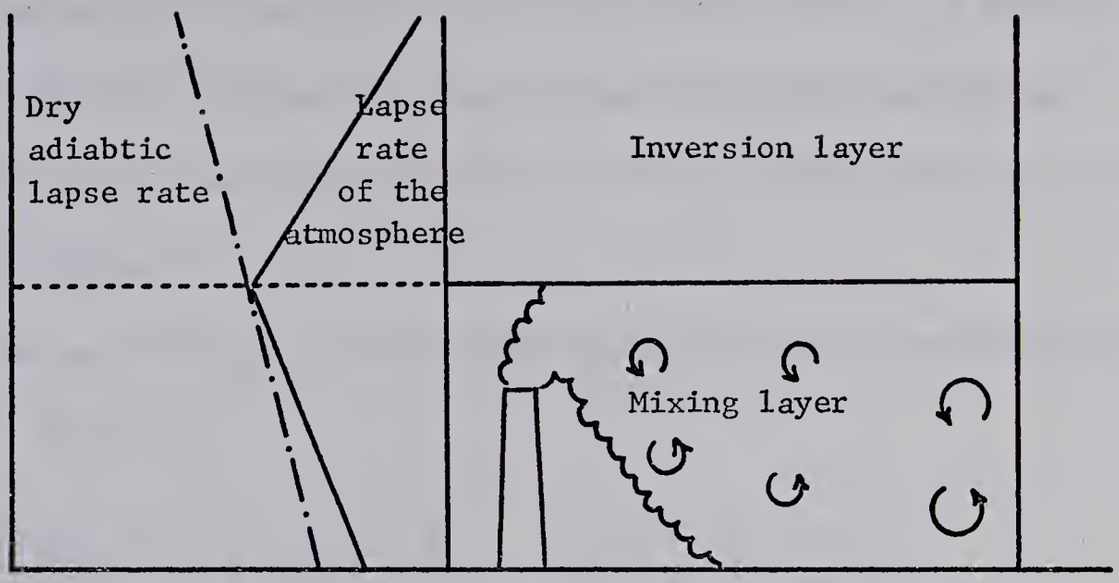

Fig. 4.4 A schematic view of the conventional box model

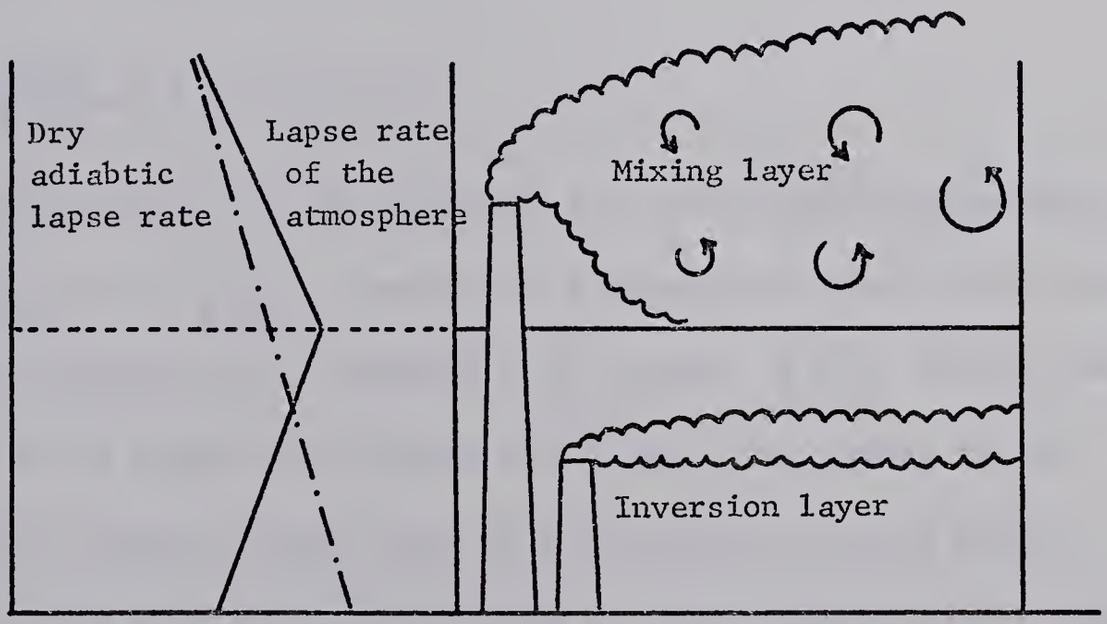

Fig. 4.5 A schematic view of the box model discussed in this research work.

The modelling equation for our study area, Box 1 , as shown in Fig. 4.2, must be modified from the original theoretical governing equation discussed in Chapter II. We will discuss these modifications in detail as follows:

(1) In Chapter II we have for the mean-state advection of pollutants in the x dimension

$$\left[\frac{\partial \bar{c}\bar{u}}{\partial x}\right] = \frac{1}{V}\left\{A_2\left[\bar{c}_2\right]_{A_2}\left[\bar{u}_2\right]_{A_2} - A_1\left[\bar{c}_1\right]_{A_1}\left[\bar{u}_1\right]_{A_1}\right\}$$

Since we set $A_1 = A_2 = A$, $V = A \times L$, and $A_1\left[\bar{c}_1\right]_{A_1}\left[\bar{u}_1\right]_{A_1} = 0$, due to the assumption that no pollutants enter Box 1 from the upwind end , the advection equation reduces to:

$$\left[\frac{\partial \bar{c}\bar{u}}{\partial x}\right] = \frac{1}{L}\left\{\left[\bar{c}_2\right]_A\left[\bar{u}_2\right]_A\right\}$$

It was impossible for us in Experiment 2 to make precise measurements of $\left[\bar{c}_2\right]_A$ and $\left[\bar{u}_2\right]_A$, because of equipment and fund limitations. However, estimates can be obtained if we express $\left[\bar{c}_2\right]_A$ as q(t), and if we assume a constant wind speed within Box 1. The latter can be obtained by taking the mean value of wind speeds at various levels. Because we are only concerned with mean pollutant concentrations, these approximations may be useable. Therefore, the above equation takes the following form:

$$\left[\frac{\partial \bar{c}\bar{u}}{\partial x}\right] = \frac{1}{L}\left[\bar{u}\right] q(t)$$

(2) There is an open boundary of Box 1 in the south-facing slope so that pollutants may enter or leave in the cross-valley direction. Therefore, we must take into consideration the advection by the y-component wind speed $[\bar{v}]$. This leads to:

$$\left[\frac{\partial \bar{c}\,\bar{v}}{\partial y}\right] = \frac{1}{L'}[\bar{v}]\; q(t) \tag{4.2}$$

(3) It was impossible also to measure $\bar{c}_1$ and $\bar{c}_2$ over horizontal planes at heights z_1 and z_2, respectively. Therefore, we must simulate these two measurements by $q_t(t)$ and $q(t)$, respectively, i.e.:

$$[\bar{c}_2]_{A_h} = q_t(t) \tag{4.3}$$

$$[\bar{c}_1]_{A_h} = q(t) \tag{4.4}$$

where $q_t(t)$ and $q_t(t)$ are time-dependent bulk values of pollutant concentrations of air in Box 2 and air in Box 1, respectively. Therefore :

$$\left[\frac{\partial \overline{c'w'}}{\partial z}\right] = \frac{-K_c(h) \cdot A_h}{h.V}\left\{q_t(t) - q(t)\right\} \tag{4.5}$$

From the above discussion, the modified modelling equation is then given as follows:

$$\frac{d\,q(t)}{dt} + \left\{\frac{[\bar{u}]}{L} + \frac{[\bar{v}]}{L'} + \frac{K_c(h).A_h}{h.V} + \frac{d\,\ln A}{d\,t}\right\} q(t) = S(t) + \frac{K_c(h).A_h.q_t(t)}{h.V} \tag{4.6}$$

In Chapter II it was shown that this equation has the solution:

$$q(t) = q_o + \left\{ \int_o^{t'} q^*(t).e^{t'}\, dt' \right\} e^{t'} \qquad (4.7)$$

If q^* is assumed to be constant for short time periods $t' = \Delta t'$ then:

$$q(t) = q_o + q^*(1 - e^{\Delta t'})\ e^{-\Delta t'} \qquad (4.8)$$

or

$$q(t) = q^* + (q^* - q_o).e^{-\Delta t'} \qquad (4.9)$$

4.3.3 Numerical equation for the governing equation

As discussed in Chapter II, in order to solve the governing equation, we have to assume that $q^*(t)$ is a constant in a short time period so that the solution of the governing equation can be treated as an initial-value problem by knowing the initial value of pollutant-concentration. If we set the calculated $q(t)$, by (4.9), as a new initial condition and assume there is a new $q^*(t)$ for this new time step then we can solve the governing equation numerically by this feedback technique. In general, we can write the numerical equation for our governing equation for any time period beginning at time t_i and ending at time $t_i + \Delta t$ as follows:

$$q_{i+1} = q^*_i + (q_i - q^*_i).e^{-\Delta t'_i} \qquad (4.10)$$

Similar to Lettau's (1970) work, representative values were assumed for source strength and for atmospheric parameters, ie., they can be provided by the field experiment work. Therefore required numerical equations for our calculation can be obtained directly from the equations obtained in Section 4.3.2. They are:

$$\frac{\bar{U}^*(t)}{L} = \frac{[\bar{u}]_i}{L} + \frac{[\bar{v}]_i}{L'} \qquad (4.11.1)$$

$$T_i^*(t) = \frac{K_{ci}(H).A_{Hi}}{V_i.H_i.} \qquad (4.11.2)$$

$$H_i^*(t) = \frac{[\ln A]_i - [\ln A]_{i-1}}{3600 \text{ sec}} \qquad (4.11.3)$$

$$f_i^*(t) = U_i^*(t) + T_i^*(t) + H_i^*(t) \tag{4.11.4}$$

$$\Delta t_i' = f_i^*(t)\Delta t \tag{4.11.5}$$

$$S_i^*(t) = S_i(t) + \frac{K_{ci}(H).A_{Hi}.q_{ti}(t)}{V_i.H_i} \tag{4.11.6}$$

$$q_i^*(t) = \frac{S_i^*(t)}{f_i^*(t)} \tag{4.11.7}$$

In our numerical calculation, the time step is taken to be 1 hour, therefore all of our data for the input to the modelling calculation have to be averaged over one-hour periods as shown in Chapters III and IV.

4.3.4 Data for the modelling computation

Two major categories of data are required by our modelling computations. They are the basic data obtained from the field experiment and derived data. The basic data were discussed in Chapter III. The derived data are discussed in this Chapter. Consider the derived data individually as follows:

1. Surface inversion height

The top of the surface-based inversion is regarded as the height of Box 1. This can be obtained from the temperature-profile measurements (Table 3.1) and the temperature measurements at Station 3. From these data we can calculate the value h_i which shows the variations of surface inversion height with time. The hourly mean heights are required by our modelling calculations. We can calculate these values for various time steps from Table 3.1. The calculated values are given in Table 4.1.

2. Temperature- and potential-temperature lapse rates

From the temperature-profile measurements, we can calculate the temperature lapse rate for Box 1 by the following equation:

$$\frac{\partial T}{\partial z}\Big|_{(z_1 \cdot z_2)^{1/2}} = \frac{T_2 - T_1}{(z_1 \cdot z_2)^{1/2} \cdot \ln(z_2/z_1)} \qquad (4.12)$$

Since most of our experimental measurements were made in a thin layer which is below a height of about 15 m above the earth surface during time steps 2000-2100 and 2300-2400, it seems reasonable to use the temperature readings at the lowest two levels to calculate the temperature

lapse rate at $(z_1.z_2)^{1/2}$. With z_1 equal to 10m and z_2 equal to 18 m, then $(z_1.z_2)^{1/2}$ is 13.4 m. Similar arguments can be applied to obtain the lapse rate during time steps 2100-2200 and 2200-2300. With z_1 equal to 18 m and z_2 equal to 26 m then $(z_1.z_2)^{1/2}$ is 21.4 m. Having temperature lapse rates, we can calculate the potential temperature lapse rates by using the equation

$$\frac{\partial \theta}{\partial z} = \frac{\theta}{T}(\gamma_d - \gamma) = (\frac{1000}{P})^{0.286}.(\gamma_d - \gamma) \qquad (4.13)$$

where P is the station surface pressure reading which can be obtained from the daily meteorological data of Edmonton Municipal Airport, and where γ_d ($0.01\,^{o}C.m^{-1}$) and γ are the dry-adiabatic lapse rate and the environment lapse rate, respectively. Because the readings of P showed little change during the time periods chosen for the modelling calculation, we may set P equal to a constant value of 938.9mb or 93890 Pa. The values of γ and $\partial\theta/\partial z$ are given in Table 4.2

Table 4.2 The temperature and potential temperature lapse rates for various time steps.

Variables	20 -21	21 - 22	22 - 23	23 - 24
γ ($^{o}C.m^{-1}$)	-0.024	-0.018	0	0.063
$\partial\theta/\partial z$ ($^{o}C.m^{-1}$)	0.035	0.029	0.01	0.038

3. Wind profile and wind shear

In this research, it is assumed that the wind profile satisfies

the power law because wind-profile measurements were not made in the Experiment 2. With this assumption, we can obtain the wind speed for any level. The data required for the calculation of the exponent of the power law are the wind speed at two appropriate levels. Using wind data for level 3.7 m and level 50 m, we can calculate the exponent from the following equation:

$$\bar{u}_{50} = \bar{u}_{3.7} \cdot \left(\frac{50}{3.7}\right)^{P_u} \tag{4.14}$$

$$\bar{v}_{50} = \bar{v}_{3.7} \cdot \left(\frac{50}{3.7}\right)^{P_v} \tag{4.15}$$

where $\bar{u}_{50}$, $\bar{u}_{3.7}$, $\bar{v}_{50}$, and $\bar{v}_{3.7}$ have been defined in Chapter III and listed in Table 3.4 and Table 3.5, and where P_u and P_v are the exponents of the power law of wind-speed components in the east-west direction and the south-north direction, respectively. The values of P_u and P_v are listed in Table 4.3.

Table 4.3 Hourly mean values of P_u and P_v for the Box 1

Exponent	Hour (MDT) 20 - 21	21 - 22	22 - 23	23 - 24
P_u	0.29	0.53	0.34	0.29
P_v	0.63	0.44	0.38	0.40

Having P_u and P_v, we can calculate the mean wind speed within Box 1 for each time step and then use the mean wind speed to calculate the mean wind speed components in the direction normal to the cross-valley

plane and in the direction parallel to the cross-valley plane. The equations for the calculation of the mean wind speed are given as follows:

$$\bar{u}_b = \frac{1}{h}\int_o^h \bar{u}_{3.7} \cdot \left(\frac{z}{3.7}\right)^{P_u} .dz \qquad (4.16)$$

$$\bar{v}_b = \frac{1}{h}\int_o^h \bar{v}_{3.7} \cdot \left(\frac{z}{3.7}\right)^{P_v} .dz \qquad (4.17)$$

where u_b and v_b are the mean wind-speed components in the east-west direction and in the north-south direction, respectively, averaged over the height of Box 1, where $\bar{u}_{3.7}$, $\bar{v}_{3.7}$ were defined in Chapter III, and where h is the height of Box 1. In addition, we can use $\bar{u}_b$ and $\bar{v}_b$ to find out the advection wind speed with respect to the directions in the cross-valley and parallel valley dimensions.They are denoted by $\bar{u}_B$ and $\bar{v}_B$, respectively. The computed mean wind components are given in Table 4.4.

Table 4.4 Hourly mean wind speed and direction with respect to geographical direction and with respect to position of Box 1.

Variables	Hour (MDT) 20 - 21	21 - 22	22 - 23	23 - 24
$\bar{u}_b$ ($m.s^{-1}$)	-2.0	-1.2	-1.4	-1.6
$\bar{v}_b$ ($m.s^{-1}$)	1.1	1.4	1.3	1.3
$\bar{V}_b$ ($m.s^{-1}$)	2.3	1.8	1.9	2.1
$\bar{u}_B$ ($m.s^{-1}$)	2.3	1.6	1.7	2.0
$\bar{v}_B$ ($m.s^{-1}$)	0.4	0.9	0.8	0.7

The procedure used for calculation of wind shear at any height z can be obtained from differentiating (4.14) and (4.15) with respect to z and the equations are given by

$$\left.\frac{\partial \bar{u}}{\partial z}\right|_z = \bar{u}_{3.7} \left.\frac{P_u}{(3.7)^{P_u}} z^{P_u-1}\right|_z \tag{4.18}$$

$$\left.\frac{\partial \bar{v}}{\partial z}\right|_z = \bar{v}_{3.7} \left.\frac{P_u}{(3.7)^{P_u}} z^{P_u-1}\right|_z \tag{4.19}$$

where we will use $z = 13.4$ m to approximate our needs. The results for various times are given in Table 4.5

Table 4.5 Wind shear within Box 1.

Wind shear (sec^{-1})	Hour (MDT)			
	20-21	21-22	22-23	23-24
$\left.\frac{\partial \bar{u}}{\partial z}\right\|_{z=13.4\ m}$	0.053	0.055	0.039	0.041
$\left.\frac{\partial \bar{v}}{\partial z}\right\|_{z=13.4\ m}$	0.074	0.052	0.042	0.050
$\left.\frac{\partial \bar{V}}{\partial z}\right\|_{z=13.4\ m}$	0.091	0.076	0.057	0.065

4. Vertical turbulent exchange coefficient K_c

It is assumed that the vertical turbulent exchange of pollutants depends solely on the turbulent exchange coefficient K_c and on the vertical gradient of pollutant concentration. We may equate the vertical turbulent exchange coefficient K_c to the thermal diffusivity K_h, ie.,

$$K_c = K_h = \frac{k.u^*.z}{\phi_h} \tag{4.20}$$

which is suggested by Panofsky (1973). Where u* is the frictional velocity which can be calculated by the equation discussed by Panofsky (1973) and is given by the equation:

$$u^* = \frac{k.z}{\phi_v} \frac{\partial u}{\partial z}$$

where k is a constant having value 0.4, z is the height above the earth surface desired for the calculation, ϕ_v is the dimensionless wind shear, and ϕ_h is the dimensionless temperature gradient. In order to calculate above mentioned variables, we require the Richardson number for various times, which can be calculated from the following equation:

$$R_i = \frac{g}{\theta} \frac{\frac{\partial \theta}{\partial z}}{(\frac{\partial V}{\partial z})^2} \qquad (4.21)$$

where g ($m.s^{-2}$) is the gravitational acceleration, and the other quantities in this equation were defined before. Accordingly, the values of R_i can be calculated by (4.21) and the results are given in Table 4.6. Having values of R_i, we can calculate the dimensionless height ζ from the following equation for the case $\zeta > 0$ which is suggested by Businger (1973) :

$$\{(4.7)^2 R_i - 4.7\}\zeta^2 + (9.4 R_i - 0.74)\zeta + R_i = 0 \qquad (4.22)$$

The calculated results of for various time are given in Table 4.6 also. Businger (1973) showed that the dimensionless temperature gradient and the dimensionless wind shear ϕ_v can be evaluted from ζ . The equations for these calculation are suggested by Businger (1973) and given by equations

$$\Phi_v = 1 + 4.7\zeta \qquad \text{for } \zeta > 0 \qquad (4.23)$$

$$\Phi_h = 0.74 + 4.7\zeta \quad \text{for} \quad \zeta > 0 \tag{4.24}$$

Having these values we can calculate u^* and K_c from (4.20) for various times. The results are given in Table 4.6.

Table 4.6 Calculated micrometeorological parameters for various times.

Variables	Hour (MDT) 20 - 21	21 - 22	22 - 23	23 - 24
Richardson number R_i	0.14	0.17	0.10	0.03
Dimensionless height ζ	0.53	1.08	0.24	0.047
Dimensionless wind shear ϕ_v	3.49	6.08	2.13	1.22
Dimensionless temperature gradient ϕ_h	3.23	5.82	1.87	0.96
Frictional velocity u^* ($m.s^{-1}$)	0.12	0.08	0.17	0.20
Exchange coefficient K_c ($m^2.s^{-1}$)	0.29	0.13	0.84	1.25

4.4 Results and discussion

The modelling calculation can be carried out by inputing the collected data, which are discussed in the previous parts of this text, to the numerical modelling equations. The results are listed in Table 4.7 and illustrated in Figs. 4.6 to 4.9.

Table 4.7 Modelling calculation results

Variables	Time step (MDT) 20 - 21	21 - 22	22 - 23	23 - 24
U*(t) (s^{-1})	0.0043	0.0039	0.0039	0.0045
T*(t) (s^{-1})	0.0011	0.0004	0.0023	0.0091
H*(t) (s^{-1})	0.0012	0.0001	0.0	-0.0002
f*(t) (s^{-1})	0.0066	0.0044	0.0062	0.013
S*(t) (ppm s^{-1})	0.0025	0.0025	0.0024	0.0031
q*(t) (ppm)	0.38	0.57	0.39	0.24
C(t) (ppm)	0.31	0.34	0.33	0.29

In Table 4.7 and Fig. 4.8 C(t) is the observed mean pollutant concentration for Box 1 obtained from the observations in Table 3.8 . $Q_1(t)$ in Fig. 4.9 is the source strength or the rate of pollutants release from the pollutant sources within Box 1. f*(t) was calculated for the time period 2000-2400 when the surface-based inversion is beginning to form. The physical meaning of f* has been discussed before. Its reciprocal is the time period in which the pollutants are transported out of Box 1 after emission from the sources. The mechanism by which the pollutants are transported out of Box 1 are advection by the

horizontal wind and vertical turbulent diffusion. Since f* is an indication of the magnitude of the transporting mechanisms, the larger the value of f* the stronger the transporting power and the shorter the time of residence of pollutants in Box 1. According to Fig. 4.6 vertical turbulent diffusion, as represented by T* (dash-dot curve), was small initially but increased later and showed much more variation than U*/L. Therefore variations in f* (solid curve), representing the sum of T* and U*/L were dominated by variations in T*. Because q*(t) is given by S*(t)/f*(t) and because S*(t) in this study has little variation with time, which can be seen from Fig. 4.7, then q*(t) may be considered to be inversely dependent on f*(t). Accordingly, the larger the value of f*(t), the smaller the value of q*(t). As noted earlier for sufficiently large values of the time step, q*(t) can be considered to be nearly equal to q(t). Therefore, we will assume $q^*(t) = q(t)$ here. Comparing the calculated pollutant concentration q(t) and the observed pollutant concentrations C(t) for each time step in Fig. 4.8 we find comparable values and similar time variations. It is of interest to compare our results with those of Panofsky (1969) who studied air pollution within a narrow valley region. He used a Gaussian diffusion model to simulate ground-level concentrations along plume centreline downwind from a source. The specific formula was:

$$C = \frac{\sqrt{2} \cdot Q}{\sqrt{\pi} \cdot V \cdot D \cdot \sigma_z}$$

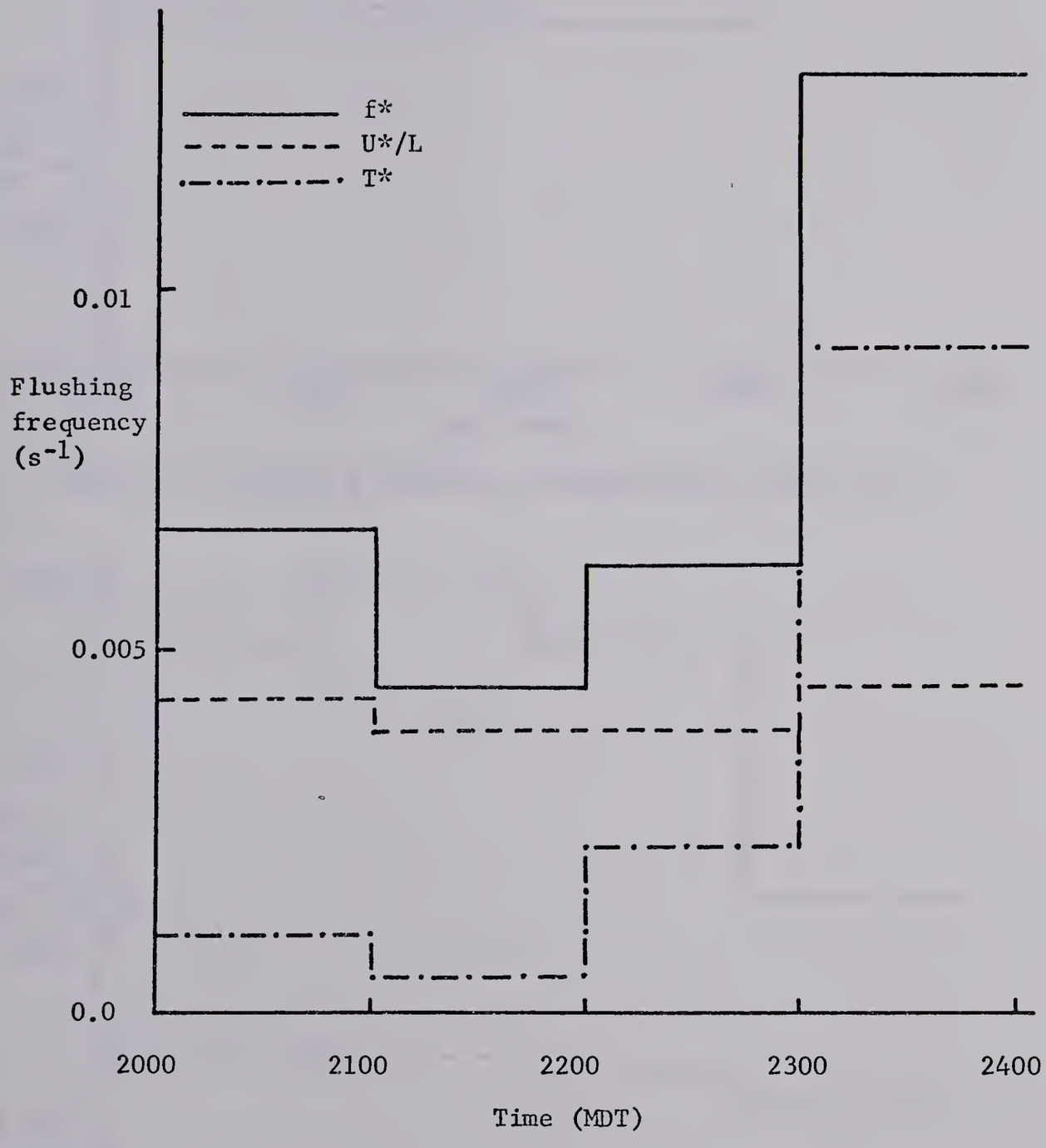

Fig. 4.6 Modelling calculation results of flushing frequencies result from horizontal advection wind speed, vertical turbulent diffusion, and total effects.

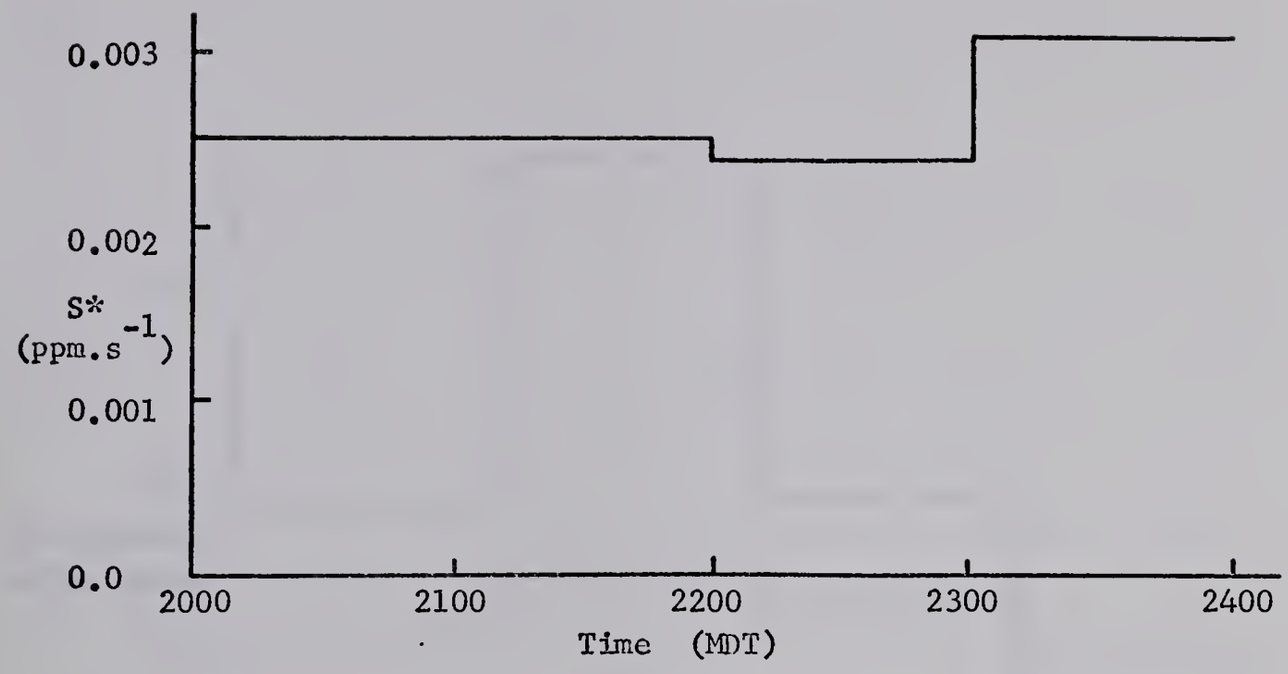

Fig. 4.7 Effective pollutant concentration within Box 1.

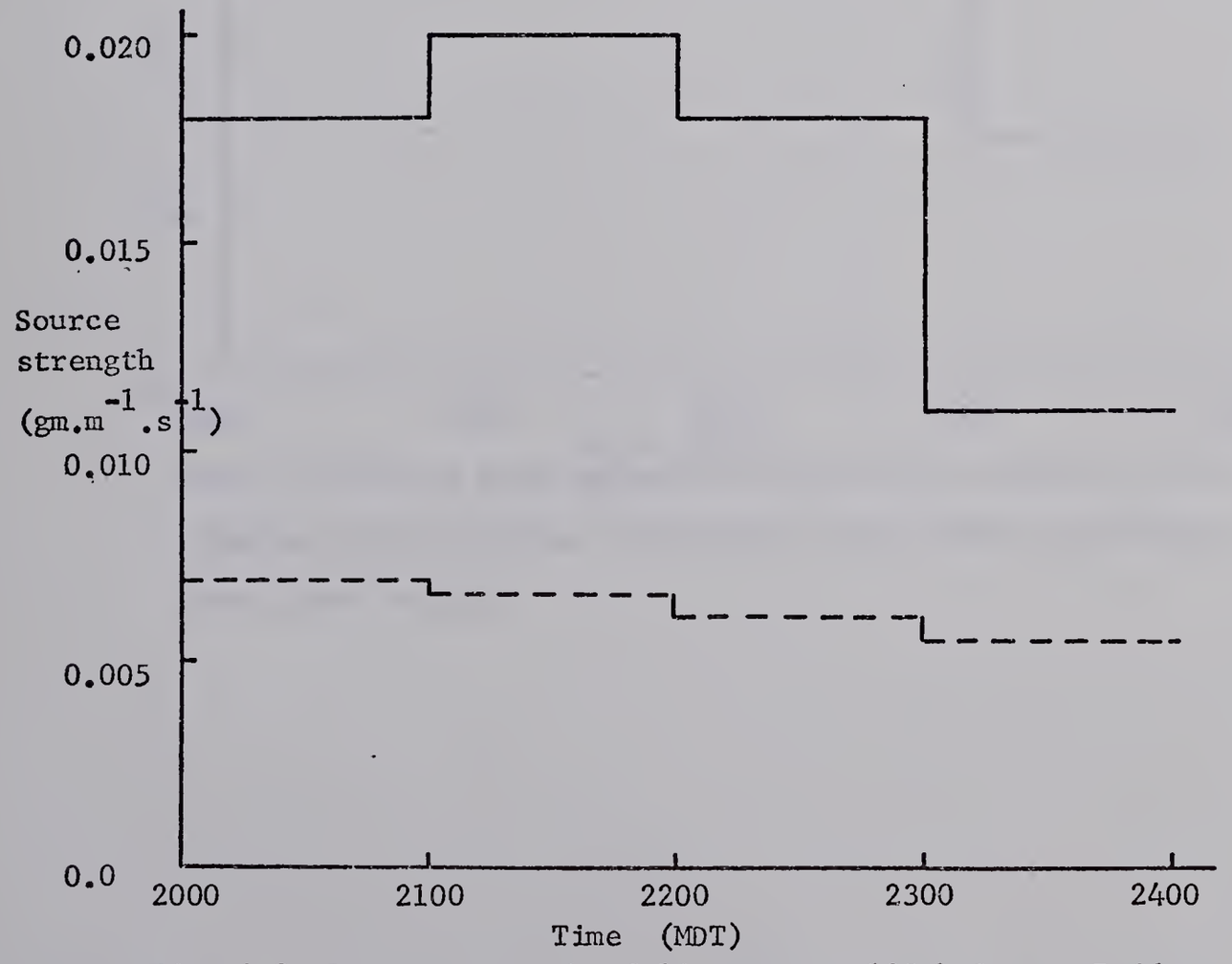

Fig. 4.8 Source strength of line source 105th Street Bridge (solid line) and line source River Valley Road (dash line).

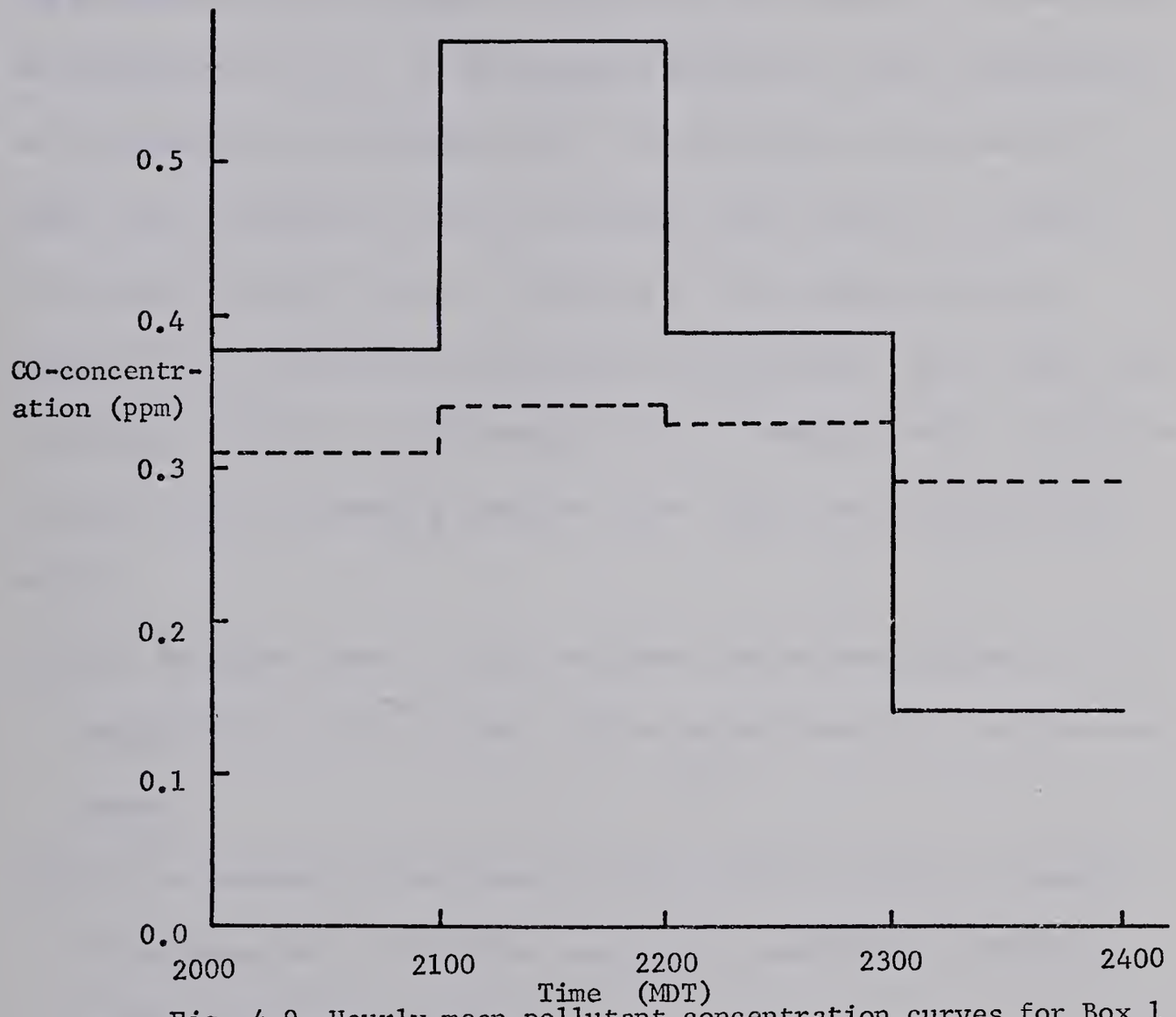

Fig. 4.9 Hourly mean pollutant concentration curves for Box 1 obtained from modelling calculation (solid curve) and observation (dash curve).

where C is the ground-level centreline pollutant concentration, Q is the pollutant source strength, V is the mean wind speed, D is the width of the valley, and σ_z is the standard deviation of mass distribution in the vertical. He indicated in the same paper that we can sum all point sources within the valley to simulate line sources or complex arrangements of point sources. According to this formula pollutant concentration is inversely proportional to wind speed, valley width, and atmospheric stability as represented by σ_z. Similar results can also be be found from our governing equation. From $q(t) = q^*(t) = s(t)/f^*(t)$, we have

(1) S(t) is proportional to Q the pollutant source strength and q(t) is proportional to S(t) so that q(t) is proportional to Q as discussed before.

(2) q(t) is inversely proportional to f*(t) which in turn is a measure of the magnitude of advection wind speed, atmospheric stability, and the dimensions of the box.

CHAPTER V

SUMMARY AND CONCLUSIONS

A review of serious air pollution episodes of the past showed that many of these took place in rather large valleys containing towns or cities and major pollution sources. Valley microclimates may have contributed significantly to the severity of these episodes. Strong nocturnal inversions can develop under clear skies in light prevailing winds and the air may stagnate in valleys resulting in poor ventilation and an accumulation of pollutants from valley sources. Downwash, inpingement, and recirculation of air in complex wind systems can also lead to local air pollution problems in valleys.

Very little is known about air pollution problems in small-scale urban valleys such as that of the North Saskatchewan River in Edmonton. One would expect that urban valley inversions at night would be more intense than those in rural portions of the valley because of the presence of the heat island above. Major roadways and bridges within the valley result in vehicle emissions that may be trapped within the valley in certain weather conditions. Trapping will be favoured by clear skies and light prevailing winds in the early evening because in such conditions vertical mixing is supressed while source strengths are still large.

A series of field experiments was undertaken in 1977 in an east-west section of the North Saskatchewan River Valley just west of the High Level Bridge in downtown Edmonton as a basis for a better understand-

ing of potential air pollution problems. In each experiment temporary weather stations were erected across the valley for small-scale measurements of wind and temperature. The meteorological measurements were supplemented by carbon monoxide traverses on both valley slopes. Detailed results of Experiment 2, which was carried out in the late afternoon and evening of July 20, 1977, are described in this thesis.

In Experiment 2 the prevailing wind above the valley was from the southeast, nearly parallel to the valley axis . Mean hourly wind speeds ranged from 3.3 to 6.1 $m.s^{-1}$ with the lowest speeds in the late evening. Southeast winds of 1.2 to 3.4 $m.s^{-1}$ were measured at valley bottom over the river. An inversion formed above the north-facing slope after 1730 LDT. It intensified steadily until 2100 LDT and then remained steady with a temperature gradient of about $12^{o}C$ per 100 m thereafter. This cold pool of air over the south bank river flats in the evening was attributed tentatively to nocturnal radiation in a shaded and sheltered location. Evidently the cool air did not spread to the north edge of the river at the gravel bar station. A shallow and rather weak inversion prevailed over the river in the evening.

Carbon monoxide concentrations were very low at all stations. The largest hourly mean values were 0.6 to 0.8 ppm near River Valley Road on the north bank. At this location concentrations declined monotonically from maximum values associated with late afternoon rush hour traffic. Away from River Valley Road but still at low elevations in the

valley carbon monoxide concentrations on both sides of the valley exhibited pronounced late evening maxima in spite of the fact that source strengths were steady or declining.

Carbon monoxide concentrations on both slopes revealed double maxima in the vertical with smaller values at intermediate heights. These maxima are thought to be due to the major upwind sources on the 105th Street Bridge and on the High Level Bridge.

A simple box model similar to that described by Lettau (1970) was applied to an east-west segment of the North Saskatchewan River Valley. The lower box contained the weak inversion layer found in the valley and the upper box enclosed less stable air above. The model involved gross spatial averaging and attempted to simulate the combined effects of time-dependent horizontal transport, vertical exchange between boxes, and pollutant emission rates. Numerous approximations were needed because of the severe limitations of the experimental data.

Predicted hourly mean carbon monoxide concentrations in the lower box were found to be comparable in magnitude to the mean values derived from traverse measurements. The pronounced evening maximum concentration predicted by the model, however, was not found in the observed spatial mean values although, as noted above, it was present at low levels on both sides of the valley. The predicted evening maximum was found to result mainly from decreasing vertical exchanges supported to a lesser extent by decreasing horizontal transport.

It is concluded that a simple two-box model can be used to obtain rough estimates of spatial mean carbon monoxide concentrations in river valley segments with known source strengths. The box model is easy to use and potentially useful for investigating time changes in pollutant concentrations that result from complex interactions between horizontal transport, vertical exchanges, and variable emission rates. However, the complexity of the valley micrometeorology as revealed in Experiment 2 is such that a fairly dense network of observation stations is needed in both horizontal and vertical directions. Only by this means can reliable spatial averages be obtained for use in the box model.

If the strong inversion that was found on the south bank flats occurred over a major thoroughfare it is possible that significantly higher pollutant concentrations would occur locally. However, an along-valley wind of 3 to 6 $m.s^{-1}$ appears to be strong enough to prevent the formation of an intense full-valley evening inversion in July.

REFERENCES

Businger, J. A.,1973: Turbulent transfer in the atmospheric surface layer, Workshop on Micrometeorology, Amer. Meteor. Soc., D. A. Haugen, Ed., 67-100.

Defant, F., 1951: Local winds, Compendium of Meteorology, Amer. Meteor. Soc., 665-672.

Davidson Ben, 1961: Valley wind phenomena and air pollution problems, J. of Air Pollution Control Assoc.,11, 363-368.

Egan, B. A., 1975: Turbulent diffusion in complex terrain, Lectures on Air Pollution and Environmental Impact Analyses, Amer. Meteor. Soc., 112-135.

Fletcher, R. D., 1949: Smog disaster - A problem in Atmospheric pollution, Weatherwise, 2, 56-60.

Firket, J., 1936: Fog along the Meuse Valley, Trans. Faraday Soc.,32, 1192-1197.

Hewson, E. W. and R. W. Longley, 1944: Slope and valley winds, Meteorology theoretical and applied, John Wiley & Sons Inc., Chapman & Hall Ltd. London, 306-310.

Hewson, E. W., 1945: The meteorological control of atmospheric pollution by heavy industry, Quart. J. Roy. Meteor. Soc., 71, 266-282.

_____, 1951: Atmospheric pollution, Compendium of Meteorology, Amer. Meteor. Soc., 1147-

Van Mieghem Jacques , 1973: Averages and fluctuations, Atmospheric Energetics, Oxford university press, 39-50.

Klassen, W., 1962: Micrometeorological observation in the North Saskatchewan River Valley at Edmonton, Meteorological Branch, Department of Transport, Technical Circular 3652, 16 pp.

Lettau, H. H., 1970: Physical and meteorological basis for mathematical models of urban diffusion processes, Pro. Symp. on Multiple-source Urban Diffusion Models, A.C. Stern, Ed, U.S. Env. Protection Agency, Publication AP-86.

Munn, R. E., 1966: The air in the valleys, Descriptive Micrometeorology, Academic Press. New York and London, 189-194.

Panofsky, H. A., 1967: The effect of meteorological factors on air pollution in a narrow valley, J. Appl. Meteor., 6, 493-499.

_____ , 1969: Air pollution meteorology, Amer. Scientist, 57, 269-285.

Pasquill, F., 1962: Atmospheric Diffusion, D. Van Nostrand Co. Ltd., Princeton, N. J.,297 pp.

Scorer, R. S., 1959: The behaviour of Chimney plumes, Int. J. Air Water Pollution, 1, 198-220.

Stern, et al, 1973: Flow through rough terrain, Fundamentals of Air Pollution, Academic Press. New York and London, 289-291.

Taylor, G. W.,1973: Automobile emission trends in Canada 1960-1985,Mobile sources Division, Abatement and Compliance Branch, Air Pollution Control Directorate, Report EPS 8-AP-73-1, 46 pp.

Tang, W., 1974: Mountain-Valley circulation and dispersion of vehicular exhaust gases from a valley highway, Symp. on Atmospheric Diffusion and Air Pollution, Santa Barbara, California, Sept. 9-13, Published by Amer. Meteor. Soc.

Yoshino, M. M., 1975: Topography and climate in a small area, Climate in a small area, University of Tokyo Press, 183-302

Zimmerman, J.R. and R. S. Thompson, 1975: Users guide for Highway, A Highway Air Pollution Model,U.S. Environmental Protection Agency, Research Triangle Park, North Carolina, Pub. No. 650/4-74-008.

APPENDIX A

EQUATION AND INFORMATIONS REQUIRES TO CALCULATE THE EMISSION FACTOR

The calculations of automotive exhaust emission factors for carbon monoxide (CO), hydrocarbon (HC), and oxides of nitrogen (NO_x) can be expressed mathematically as:

$$E_{np} = \sum_{i=n-8}^{n} L_{ip} \cdot d_{ipn} \cdot W \cdot M_{in} + \sum_{i=n-8}^{n} (C_i \cdot V + h_i) \cdot M_{in}$$

where E_{np} is the emission factor in grams per vehicle-mile for calendar year n and pollutant p, L_{ip} is the 1972 'Federal' test procedure emission rate for pollutant p (gram.mile^{-1}) for the ith model year at low milage, d_{ipn} is the vehicle pollutant p emission deterioration factor for the ith model year at calendar year n, M_{in} is the weighted annual travel of the ith model year during calendar year n (the determination of the variable involves the use of the vehicle model year distribution), W is the cold weather weighting factor for exhaust pollutants (1.3), C_i is the evaporative emission rate for the ith model year, V is the cold weather weighting for evaporative emissions (0.5), and h_i is the crank-case emission rate in the ith model year. The required information for the calculation follows Taylor (1973) and is given as follows:

Table A-1 Canadian vehicle age distribution.(Source: R. L. Polk (Canada) Co. Ltd.)

Vehicle age (Years) from end of model year (Oct. 1)	Vehicle population as of July 1 (o/o)	Vehicle population by full model year (o/o)
0	8.6	10.5
1	11.8	11.5
2	12.4	12.1
3	11.7	11.5
4	10.8	10.6
5	8.5	8.3
6	7.4	7.2
7	5.9	5.7
8	5.3	5.2
> 8	17.6	17.4

Table A-2 Percentage of annual vehicles travelled by different age groups.

Vehicle age (Years)	Total annual vehicle miles (o/o)
1	15.73
2	13.64
3	12.02
4	10.07
5	9.35
6	8.18
7	7.50
8	23.50

Table A-3 Average new car emission rates in Canada as a function of model year

Model year	Hydrocarbon ($g.mile^{-1}$) Exhaust L_{ip}	Blowby h_i	Evaporation C_i	Carbon Monoxide ($g.mile^{-1}$) L_{ip}	oxides of nitrogen ($g.mile^{-1}$)
pre-1963	17	4.08	2.77	125	3.6
1963	17	0.82	2.77	125	3.6
1964	17	0.82	2.77	125	3.6
1965	17	0.82	2.77	125	3.6
1966	17	0.82	2.77	125	3.6
1967	17	0.82	2.77	125	3.6
1968	7.0	0.00	2.77	71	4.3
1969	7.0	0.00	2.77	71	5.5
1970	4.6	0.00	2.77	47	5.1
1971	4.6	0.00	2.77	47	4.8
1972	3.4	0.00	0.14	39	4.6
1973	3.4	0.00	0.14	39	2.3
1974	3.4	0.00	0.14	39	2.3
1975	0.45	0.00	0.14	4.7	2.3
1976 and late	0.45	0.00	0.14	4.7	0.31

Table A-4 Average vehicle emission degradation factors

Pollutant	Vehicle age (years)	Model year 1967	1968	1969	1970 and late
HC	0 - 1	1.00	1.00	1.00	1.00
	1 - 2	1.17	1.17	1.12	1.00
	2 - 3	1.36	1.28	1.20	1.21
	3 - 4	1.44	1.37	1.28	1.24
	4 - 5	1.50	1.43	1.30	1.28
	5 - 6	1.55	1.53	1.34	1.31
	6 -	1.57	1.53	1.34	1.33
CO	0 - 1	1.00	1.00	1.00	1.00
	1 - 2	1.21	1.50	1.21	1.27
	2 - 3	1.37	1.82	1.35	1.47
	3 - 4	1.49	2.03	1.45	1.61
	4 - 5	1.54	2.17	1.52	1.70
	5 - 6	1.57	2.25	1.55	1.76
	6 -	1.58	2.28	1.56	1.78
NO_x	A degradation of 1.00 was used for all model years throughout their lifetime